DOKUZ EYLÜL UNIVERSITY
GRADUATE SCHOOL OF NATURAL AND APPLIED SCIENCES

NUMERICAL SOLUTION OF TWO DIMENSIONAL PHASE CHANGE PROBLEM INVOLVING NATURAL CONVECTION

by
Mustafa KALFA

August, 2017
İZMİR

NUMERICAL SOLUTION OF TWO DIMENSIONAL PHASE CHANGE PROBLEM INVOLVING NATURAL CONVECTION

A Thesis Submitted to the
Graduate School of Natural and Applied Sciences of Dokuz Eylül University
in Partial Fulfillment of the Requirements for the Degree of Master of Science
in Mechanical Engineering, Thermodynamics Program

by

Mustafa KALFA

August, 2017

İZMİR

M.Sc THESIS EXAMINATION RESULT FORM

We have read the thesis entitled **"NUMERICAL SOLUTION OF TWO DIMENSIONAL PHASE CHANGE PROBLEM INVOLVING NATURAL CONVECTION"** completed by **MUSTAFA KALFA** under supervision of **ASST. PROF. DR. MEHMET AKİF EZAN**and we certify that in our opinion it is fully adequate, in scope and quality, asa thesis for the degree of Master of Science.

Asst. Prof. Dr. Mehmet Akif EZAN

Supervisor

Prof. Dr. Aytunç EREK

(Jury Member)

Asst. Prof. Dr. Mustafa ASKER

(Jury Member)

Prof. Dr. Emine İlknurCÖCEN

Director

Graduate School of Natural and Applied Sciences

ACKNOWLEDGEMENTS

First of all, I wish to express my sincere gratitude to my advisor, Asst. Prof. Dr. Mehmet Akif EZAN, for providing excellent guidance, continuous support, friendly attitude and constant encouragement throughout the preparation of this thesis. His contribution to the achievements of this work is significant. It has been an honor for me to be able to work with him.

I also would like to thank Prof. Dr. Aytunç EREK, for motivating me about CFD and bring us together with Dr. EZAN.

Finally, I would like to express my deepest gratitude to my dearest family, especially my sister Beste KALFA for standing beside me all of my life. I would also like to thank my precious friend Merve ALTIN for her support and motivation during the process. I feel so special to have all of them.

Mustafa KALFA

NUMERICAL SOLUTION OF TWO DIMENSIONAL PHASE CHANGE PROBLEM INVOLVING NATURAL CONVECTION

ABSTRACT

This study mainly focuses on the numerical solution of two different types of natural convection problems. The first problem indicates the transient heat transfer process inside a two-dimensional cavity. The numerical model has been created with a control volume approach by using C plus plus. In order to determine the accuracy of the numerical code, comparisons are made with the results of the numerical analyses and experimental velocity measurements from the literature. After that, the time-dependent variations of local and average Nusselt numbers have been revealed for various aspect ratios and different thermal boundary conditions of the cavity. The interaction of temperature and velocity distributions by different boundary conditions has been examined. The other problem includes the transient heat transfer process of freezing of water inside a two-dimensional square cavity. Water is used as a phase-change medium, and the numerical model has been created with control volume approach by using C plus plus. To be able to accelerate the numerical calculations, CUT (Consistent Update Technique) algorithm is implemented in the numerical code. Spanwise variations of the vertical component of the velocity are represented in comparison with the experimental measurements from the literature at various vertical positions to examine the accuracy of the numerical scheme. Four different solidification scenarios are tested by cooling from the side, bottom and top walls. The influence of natural convection during the process is considered by comparing the conduction and convection dominated solidification under the same boundary conditions. The effect of overall heat transfer coefficient is also examined by various convective heat transfer coefficients of the wall and thermal conductivities of the wall material. The streamlines and isotherms are also represented to understand the differences between the conduction and convection driven phase change processes.

Keywords: Transient natural convection, density inversion, phase change, CUT

DOĞAL TAŞINIM İÇEREN İKİ BOYUTLU FAZ DEĞİŞİM PROBLEMİNİN SAYISAL ÇÖZÜMÜ

ÖZ

Bu çalışmada, iki farklı doğal taşınım probleminin sayısal çözümü üzerinde durulmuştur. İlk problem, iki boyutlu bir kavite içindeki zamana bağlı ısı transferi sürecini göstermektedir. Sayısal model, C plus plus programlama dili kullanılarak kontrol hacimleri yaklaşımı ile oluşturulmuştur. Geliştirilen kodun doğruluğunu saptamak için sayısal analiz sonuçları ve literatürdeki deneysel hız ölçümleri karşılaştırılmıştır. Ayrıca, çeşitli en-boy oranları ve farklı ısıl sınır koşulları altında yerel ve ortalama Nusselt sayılarının zamana bağlı değişimleri gösterilmiştir. Sıcaklık ve hız dağılımlarının farklı sınır koşulları ile etkileşimleri de incelenmiştir. Diğer problem ise, iki boyutlu kare kavite içerisinde dondurulan suyun zamana bağlı ısı transferi sürecini içermektedir. Faz değişim malzemesi olarak su kullanılmıştır ve sayısal model, kontrol hacimleri yaklaşımı ile C plus plus kullanılarak oluşturulmuştur. Hesaplamaları hızlandırmak için sayısal koda CUT (Consistent Update Technique) algoritması uygulanmıştır. Hızın düşey bileşeninde boylu boyunca oluşan dalgalanmalar, literatürdeki deneysel ölçümlerle karşılaştırılarak sayısal kodun doğruluğu ispatlanmıştır. Yanlardan, alttan ve üstten olmak üzere dört farklı katılaşma senaryosu ile çalışılmıştır. Aynı sınır koşulları altında, iletim ve taşınımın baskın olduğu durumlar karşılaştırılarak doğal taşınımın faz değişim sürecine etkisi incelenmiştir. Duvarların ısıl iletkenliği ve ısı transfer katsayıları değiştirilerek genel ısı transferi katsayısının sürece etkisi gözlemlenmiştir. Faz değişimi boyunca iletim ve taşınımın baskın olduğu durumlar arasındaki farkın anlaşılması için ise, belli zamanlardaki akış çizgileri ve izoterm eğrileri gösterilmiştir.

Anahtar kelimeler: Zamana bağlı doğal taşınım, yoğunluk dönüşümü, faz değişimi, CUT

CONTENTS

Page

LIST OF FIGURES

Page

LIST OF TABLES

Page

CHAPTER ONE
INTRODUCTION

1.1 Introduction

Natural (or *free*) convection is a buoyancy-driven heat transfer mechanism that occurs in fluids and governed by the temperature difference. It is the most widely used mode of heat transfer due to its low maintenance, low cost and low possibility of resonance. It is widely encountered in thermal systems such as heating/cooling of buildings, drying of foods, thermal control of electronic devices, convection in combustion chambers, safety of reactors, and energy storage involving a phase change (solid/liquid). The temperature variations inside the fluid cause the density differences so that natural fluid motion occurs. Boussinesq approximation can be validly used to investigate the natural convection of the fluids that have linear density variations with respect to the temperature, such as air (Bergman, Incropera & Lavine, 2011). On the other hand, the density variations of some liquids (i.e. water, gallium, and tellurium) are not defined linearly by temperature. After a certain temperature, the density variations become reversely proportional to increasing temperature. As an instance, the density of water increases with the temperature range of 0°C to 4°C. After 4°C, its density decreases with increasing temperature. Hence, 4°C is known as "*density inversion*" point in the literature (Seki, 1978; Inaba & Fukuda, 1984; Lin & Nansteel, 1987).

In Figure 1.1, three different cavities are illustrated to discuss the effect of density variations of water on natural convection. Here, the temperature of the right-hand side wall is kept as T_H, and the left one is also held as T_C. Under the steady-state condition, the flow structure inside the cavity is related to *density inversion* parameter (R).

$$R = \frac{T_m - T_c}{T_H - T_c} \tag{1.1}$$

where, T_m represents the temperature at a maximum density (for water $T_m = 4°C$). For $R < 0$ ($T_H > T_C > T_m$), the density of the fluid in the cavity is increased from hot wall to cold wall. Therefore, a counter-clockwise single circulation cell is obtained inside the cavity (Figure 1a). For $R > 0$ ($T_m > T_H > T_C$), density is increased from cold wall to hot wall, so that, a clockwise single circulation cell is obtained inside the cavity (Figure 1b). On the other hand, for $0 < R < 1$ ($T_H > T_m > T_C$), density is increased from cold wall to hot wall, and it reaches the maximum value at T_m, beyond that point the density decreases. Thus, the flow structure inside the cavity is divided into two regions on T_m. While the clockwise rotated circulation cell occurs on the left-hand side of the point T_m, the counter-clockwise cell is observed at the other part of the cavity (Figure 1.1c).

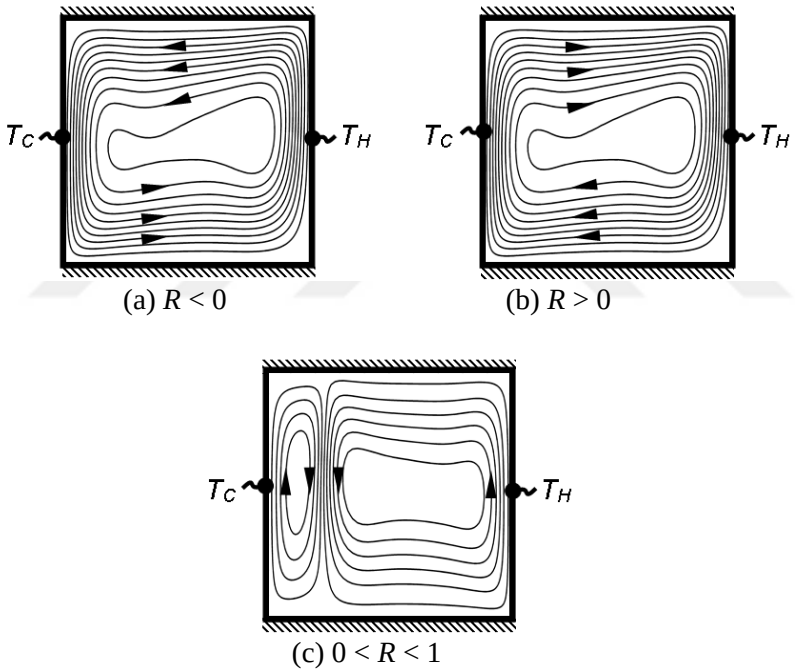

(a) $R < 0$ (b) $R > 0$

(c) $0 < R < 1$

Figure 1.1 Effect of density inversion parameter on natural convection

A dynamic flow and a heat transfer of transient natural convection in cavities have been extensively studied in an effort to develop models to simulate physical phenomena realistically. It is important to understand heat and species transport process in order to minimize unwanted convective flow during melting processing and other applications.

In literature, the studies that have been conducted on the natural convection of water can be divided into two parts; *(i) steady state* and *(ii) transient*. However, transient natural convection received little attention before the 1980s, and the transient behavior of flowmotion was rarely documented. The majority of work on natural convection in enclosures focused on the steady state behavior, for instance, two vertical walls are maintained at constant but different temperatures or heat flux. However, in most applications, the thermal boundary conditions cannot be treated as steady due to the changing ambient environment. Thus, transient or unsteady convection occurs. The earliest attempt to study the unsteady natural convection is through step change temperatures on sidewalls.

Natural convection in cavities has been examined both numerically and experimentally by various researchers. Earliest work in simulation of the natural convection of laminar flow in square enclosures is reported by DeVahl & Davis (1983), and DeVahl, Davis & Jones (1983). They acquired the solutions of the equations characterizing laminar natural convection in 2D square cavity which has differentially heated side walls for Ra 10^3 to 10^6. Seki (1978) investigated steady-state natural convection both numerically and experimentally in rectangular vessels that have various temperature differences and aspect ratios (H/W = 1 and H/W = 5). They have stated that unlike common fluids that have linear density-temperature relationships, for the case of water, the average Nusselt number is a peculiar function of temperature difference between the side walls. Inaba & Fukuda (1984) analyzed the flow and temperature distribution of water inside an inclined cavity for different angles. Lin & Nansteel (1987) developed a numerical model of natural convection inside the square cavity for different Rayleigh numbers (Ra = 10^3 to 10^6) and density inversion parameters (R = 0.4, 1/2, 0.55, 2/3, 3/4 and 1). Hossain & Rees (2005) observed the steady-state natural convection inside a cavity for different aspect ratios driven by uniform heat generation. Braga & Viskanta (1992) and McDonough & Faghri (1994) investigated the transient heat transfer of the cavity filled with water both numerically and experimentally. Helium-neon laser and pH-indicator methods are used to visualize the flow structures, respectively. The velocity distributions are presented based on various temperature differences inside the cavity. Wei & Koster

(1994) studied transient natural convection inside cavities with different aspect ratios and temperature differences. Banaszek, Jaluria, Kowalewski & Rebow (1999) developed a semi-closed finite element method to investigate phase change problems including both convection and conduction effects of heat transfer. Transient heat transfer of water inside a square cavity is observed by using PIV (Particle-Image-Velocimetry) method to order to validate the accuracy of the numerical model. In experiments, one side of the cavity is kept at 10°C, and the other side is held at -10°C (or 0°C) to observe natural convection with (or *without*) phase change. Moraga & Vega (2004) generated two and three-dimensional models of the natural convection problem that has been already studied by Banaszek et al. (1999). They revealed the difference between those two models. Recently, Kandaswamy, Sivasankaran & Nithyadevi (2007), and Nithyadevi, Kandaswamy & Lee (2007) investigated transient natural convection of water in a cavity with partially active vertical walls. They have developed a numerical code with considering that, except density, the fluid properties are constant. Time-wise variations of average Nusselt numbers and velocity/temperature distributions are obtained for various aspect ratios of the cavity. Lankford & Bejan (1982) carried out some experiments in a vertical enclosure where a constant heat flux boundary condition was put into practice on the vertical hot wall while the other wall was cooled down. Yewell, Poulikakos & Bejan (1982) explored transient natural convection in an enclosure with low-aspect-ratios (H/W = 0.0625 and H/W = 0.112) and high Rayleigh numbers. They chose water as a running fluid between 15 and 35°C, where the density inversion does not take place. Ho & Viskanta (1984) noticed the primary solid-liquid interface data during the phase change process of *n*-octadecane in a 2D rectangular cavity with vertically conducted walls. The heating or cooling of the cavity was occurred through the bottom wall. They accomplished that for solid-liquid phase change heat transfer, short surfaces are more effective than longer ones. Hale & Viskanta (1984) established the motion between solid-liquid interface during the freezing and melting processes from top and down of several different substances (*not including water*) in a rectangular cavity. Only a few papers were found in which the freezing of water had been investigated in the literature. Cheng, Inaba & Gilpin (1988) used water as a running fluid in order to investigate the effect of natural convection on ice formation around a

cold isothermal horizontal cylinder. The Nusselt number at stagnation point, the local heat transfer coefficient, and the average Nusselt number behavior at the ice/water interface were practiced. Flow reversions caused by the existence of the density extension of water at 4°C affected seriously the heat transfer at the ice/water front besides the development of this front. Chellaiah & Viskanta (1989) worked on the transient freezing process of superheated water-porous media in a rectangular enclosure both experimentally and numerically. They observed the effect of horizontal temperature difference between two vertical walls of an enclosure that is initially filled with isothermal and motionless fluid. Sugawara, Inaba & Seki (1988) also worked with a water-filled porous layer. They achieved a transient experiment where the top-cold wall was maintained at −20°C while the lower-hot wall was maintained between 0 and 30°C. It was certainly found on these experiments that the density inversion of water affects both the convective motion and the solidification process. Borger and Westwater (1967) had calculated interface velocities and temperature profiles during the freezing of water and the melting of ice in a rectangular cavity which made of adiabatic vertical walls and heated or cooled horizontal walls. At the highest Rayleigh number took place, oscillations in the interface velocity had been declared. Chu, Churchill & Patterson (1976) performed some computational analysis about the effect of heater size, heater location, aspect ratio and boundary condition on 2D rectangular ducts. Turkoglu & Yucel (1995) explored the effects of the partially heated and cooled side walls on natural convection heat transfer in Cartesian cavities. They created a numerical model to conjecture the flow and temperature fields in the cavity. Valencia & Frederick (1989) had studied numerically the heat transfer in a square enclosure with partly active vertical walls for Rayleigh numbers 10^3 and 10^7 investigating five different locations of an active source. Zhao, Liu & Tang (2007) performed both theoretical and numerical analysis about the transient flow of two heated elements under time-dependent temperature conditions in a square geometry. Deng (2008) improved the numerical examination on natural convection heat transfer in square enclosure owing to two and three separated heat source (sink) pairs placed on the vertical side walls. Cheikh, Beya & Lili (2007) had a numerical work on natural convection heat transfer in a square cavity with a discrete heat source from below and cooling from above

under several thermal boundary conditions of top and side walls. Zaman, Turja & Molla (2013) numerically studied the natural convection heat transfer of an airflow in a Cartesian cavity with two different heat sources from below for Rayleigh numbers 10^3 and 10^7. Chen & L.Y. Chen (2007) developed a numerical simulation of natural convection heat transfer in a square cavity with discrete heat sources on the left and on the bottom walls for Rayleigh numbers 10^2 and 10^7. Sharif & Mohammad (2005) completed a numerical research on natural convection in geometries with constant heated flux at the bottom wall and isothermally cooled flux at the side wall. Wu & Ching (2010) worked an experiment on the natural convection heat transfer in a square cavity with a horizontal part of two different lengths attached to the heated vertical wall in two different positions. Muralidhar, Patil & Kashyap (1995) explored an interferometric study on transient natural convection in an enclosure for three different Rayleigh numbers. Balaszcuk (2013) had an experimental study about natural convection heat transfer for different inclination angles and different thermal conditions of heating surfaces in a converging duct. Shiralkar, Gadgil & Tien (1981) investigated a natural convection in shallow horizontal cavities which have different temperatures of adiabatic horizontal walls and isothermal vertical walls for high *Ra* numbers ($> 10^6$). They realized that the boundary layers covering both the vertical and the horizontal walls diverge qualitatively from the flow regime of low *Ra* numbers where the horizontal boundary layers were unavailable. They recommended a new correlation for the Nusselt number in that kind of flow regime. Ravi, Henkes & Hoogendoom (1994) studied on a 2D natural convective flow in an enclosure with adiabatic horizontal walls and isothermal vertical walls kept at a certain temperature difference for *Ra* numbers varying from 10^4 to 10^8. They observed that, at high *Ra* numbers, a recirculating pouch has come in sight near the lower corners of the vertical walls. The flow is separated and then reattached at the horizontal walls at the surroundings of this recirculation. They accomplished that the corner flow and the transition region were not due to the hydraulic jump theory. Fusegi & Hyun (1994) were reported some studies about naturally convective flows in a cavity with heated side walls. They emphasized the inconsistencies between the 2D numerical predictions with idealized boundary conditions and the suitable experimental measurements. They also discussed about four main affairs (finiteness of thermal

conductance of the solid walls, variable physical properties of the fluid, time-dependent thermal loading, and the three dimensionalities) that need to be addressed in the conventional way of simulation to make it more realistic.

This research study was motivated by understanding the development of a flow structure and a capacity of thermal energy storage of water under different boundary conditions during solidification. A numerical code is developed in which temperature dependent thermo-physical properties of water are taken into account. The validity of the code is proved by reproducing a natural convection problem from the literature. Calculations were executed in a two-dimensional square cavity to work the transient flow in a fluid (which is initially isothermal and motionless) due to a bit decrease in temperature on a specified wall. In analyzes, water has been chosen as the phase-change medium where the cold wall temperature was fixed below the freezing temperature of water. Heat gain was defined through the insulated walls under certain ambient temperature and convective heat transfer coefficient. Water was maintained at 4°C (density extremum temperature). The growing of ice and the transient flow in the cavity were monitored by the numerical method to examine the effect of the cold wall that has different positions, and overall heat transfer coefficients. It was found that the overall heat transfer coefficient of water strongly effects the growing of ice and convective flow in the liquid region of the cavity. Time-wise and space-wise variations of local and average Nusselt numbers are also investigated for different aspect ratios of the cavity and several thermal boundary conditions.

CHAPTER TWO
SOLUTION METHODS

2.1 Definition of Solution Methods

2.1.1 Generation of Mesh

In order to analyze fluid flows, flow domains must be divided by smaller subdomains. The governing equations are then discretized and solved inside each of the subdomains. Typically, there are three methods to solve the approximate version of the system of equations: finite volumes, finite elements, or finite differences. Serious attention must be taken to provide a proper continuity of solution across the common interfaces between two subdomains so that the approximate solutions inside various portions can be put together to give a complete picture of fluid flow in the entire domain. The subdomains are often called elements or cells, and the collection of all elements or cells is called a mesh or grid. Figure 2.1 represents a two-dimensional analysis domain and its mesh.

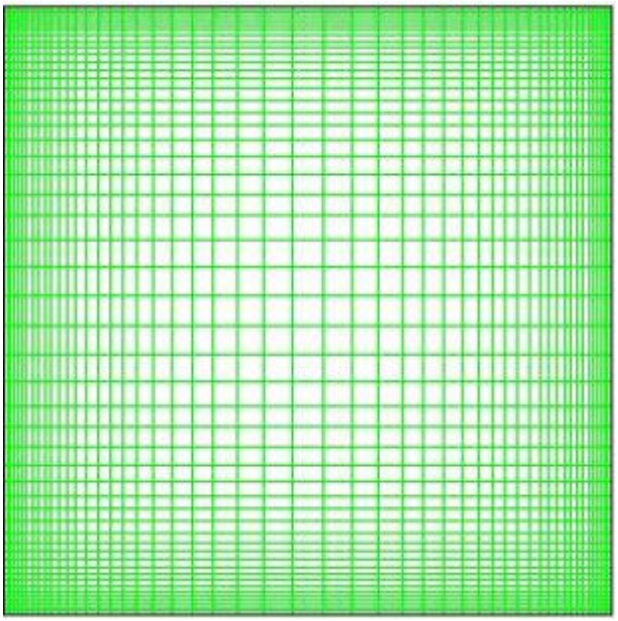

Figure 2.1 Generation of mesh inside a cavity

2.1.2 Finite Volume Method

Finite volume method (FVM) is a discretization technique for partial differential equations in the form of algebraic equations. Values are calculated at separate parts on a meshed geometry. Finite volume refers to the small volume surrounding each node point on a mesh. In this method, volume integrals in a partial differential equation that contain a divergence term are converted to surface integrals by using the divergence theorem. These terms are then evaluated as fluxes at the surfaces of each finite volume. Because the flux entering a specified volume is identical to that leaving the adjacent volume, these methods are conservative. Another advantage of the finite volume method is that it is formulated to allow for unstructured meshes easily (Versteeg & Malalasekara, 1995).

General form of two-dimensional convection-diffusion equation is given below

$$\frac{\partial}{\partial t}(\rho\phi)+\frac{\partial J_x}{\partial x}+\frac{\partial J_y}{\partial y}=S \tag{2.1}$$

where J_x and J_y are the total (*convection plus diffusion*) fluxes defined by

$$J_x \equiv \rho u\phi-\Gamma\frac{\partial\phi}{\partial x} \tag{2.2}$$

$$J_y \equiv \rho v\phi-\Gamma\frac{\partial\phi}{\partial y} \tag{2.3}$$

where u and v denote the velocity components in the x and y-directions. The integration of Equation 2.1 over the control volume shown in Figure 2.2 would give

$$\frac{\left(\rho_P\phi_P-\rho_P^0\phi_P^0\right)\Delta x\Delta y}{\Delta t}+J_e-J_w+J_n-J_s=\left(S_C+S_P\phi_P\right)\Delta x\Delta y \tag{2.4}$$

where the source term has been linearized in the usual manner and, for the unsteady term, ρ_P and ϕ_P are assumed to prevail over the whole control volume. The old values (the values at the beginning of the time step) are denoted by ρ_P^0 and ϕ_P^0.

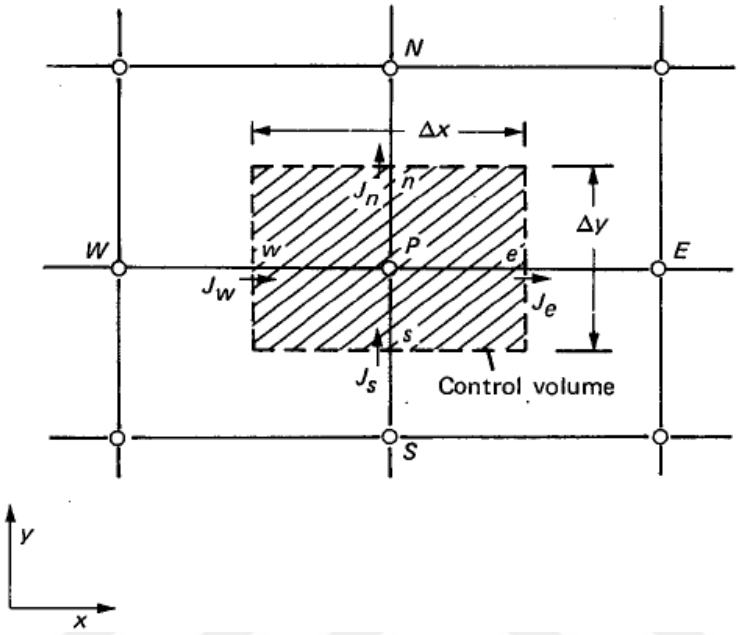

Figure 2.2 Control volume for two-dimensional situation (Patankar, 1980)

In conformity with the fully implicit practice, all other values (those without a superscript) are to be regarded as new values. J_e, J_w, J_n, and J_s are the integrated total fluxes over the control volume faces (J_e refers $\int J_x dy$ over the interface *e*, and so on).

In a similar manner, two-dimensional form of continuity equation which is integrated over control volume is given as

$$\frac{\left(\rho_P - \rho_P^0\right)\Delta x \Delta y}{\Delta t} + F_e - F_w + F_n - F_s = 0 \tag{2.5}$$

where F_e, F_w, F_n, and F_s are the mass flow rates through the faces of the control volume. If ρu at point *e* is taken to prevail over the whole interface *e*,

$$F_e = (\rho u)_e \, \Delta y \tag{2.6}$$

$$F_w = (\rho u)_w \, \Delta y \tag{2.7}$$

$$F_n = (\rho u)_n \, \Delta x \tag{2.8}$$

$$F_s = (\rho u)_s \, \Delta x \tag{2.9}$$

Then,

$$(\phi_P - \phi_P^0)\frac{\rho_P^0 \Delta x \Delta y}{\Delta t} + (J_e - F_e\phi_P) - (J_w - F_w\phi_P) + (J_n - F_n\phi_P) - (J_s - F_s\phi_P) = (S_C + S_P\phi_P)\Delta x \Delta y \tag{2.10}$$

$$J_e - F_e\phi_P = a_E(\phi_P - \phi_E) \tag{2.11}$$

$$J_w - F_w\phi_P = a_W(\phi_W - \phi_P) \tag{2.12}$$

where,

$$a_E = D_e A(|P_e|) + \S F_e, 0^{\cdot\cdot} \tag{2.13}$$

$$a_W = D_w A(|P_w|) + \S F_w, 0^{\cdot\cdot} \tag{2.14}$$

Here D_e and D_w, like their counterparts F_e and F_w, contain the area Δy of the faces *e* and *w*. Similar expressions for $J_n - F_n\phi_P$ and $J_s - F_s\phi_P$ can be written.

The final discretization equation now can be written as

$$a_P f_P = a_E f_E + a_W f_W + a_N f_N + a_S f_S + b \tag{2.15}$$

$$a_E = D_e A(|P_e|) + [\,F_e, 0] \tag{2.16}$$

$$a_W = D_w A(|P_w|) + [F_w, 0] \tag{2.17}$$

$$a_N = D_n A(|P_n|) + [\,F_n, 0] \tag{2.18}$$

$$a_S = D_s A(|P_s|) + [F_s, 0] \tag{2.19}$$

$$a_P^0 = \frac{r_P^0 \Delta x \Delta y}{\Delta t} \tag{2.20}$$

$$b = S_C \Delta x \Delta y + a_P^0 f_P^0 \tag{2.21}$$

$$a_P = a_E + a_W + a_N + a_S + a_P^0 - S_P \Delta x \Delta y \tag{2.22}$$

Here ϕ_P^0 and ρ_P^0 refer to the known values at a time *t*, while all other values ate the unknown values at a time $t + \Delta t$. The corresponding conductances are defined by

$$D_e = \frac{\Gamma_e \Delta y}{(\delta x)_e} \tag{2.23}$$

$$D_w = \frac{\Gamma_w \Delta y}{(\delta x)_w} \tag{2.24}$$

$$D_n = \frac{\Gamma_n \Delta y}{(\delta x)_n} \tag{2.25}$$

$$D_s = \frac{\Gamma_s \Delta y}{(\delta x)_s} \tag{2.26}$$

Peclet numbers by

$$P_e = \frac{F_e}{D_e} \tag{2.27}$$

$$P_w = \frac{F_w}{D_w} \tag{2.28}$$

$$P_n = \frac{F_n}{D_n} \tag{2.29}$$

$$P_s = \frac{F_s}{D_s} \tag{2.30}$$

Power Law scheme is selected in this study. Because it is more efficient and is preferred by Patankar, 1980. So, the function $A(|P|)$ is defined as

$$A(|P|) = \begin{cases} 0, & (1 - 0.1|P|)^5 \end{cases} \tag{2.31}$$

2.1.3 Harmonic Mean Interpolation

When the diffusion coefficients of the control volume centroids (Γ_P, Γ_E, Γ_W, Γ_N, Γ_S) are known, the diffusion coefficients of the control volume faces (Γ_e, Γ_w, Γ_n, Γ_s) are to be calculated by using harmonic mean interpolation rather than the arithmetic mean interpolation.

$$\Gamma_e = \frac{2\Gamma_P \Gamma_E}{\Gamma_P + \Gamma_E} \tag{2.32}$$

$$\Gamma_w = \frac{2\Gamma_P \Gamma_W}{\Gamma_P + \Gamma_W} \tag{2.33}$$

$$\Gamma_n = \frac{2\Gamma_P \Gamma_N}{\Gamma_P + \Gamma_N} \tag{2.34}$$

$$\Gamma_s = \frac{2\Gamma_P \Gamma_S}{\Gamma_P + \Gamma_S} \tag{2.35}$$

The harmonic mean interpolation has an important advantage, especially for multi-dimensional problems. With this type of interpolation, nothing special need to be done when treating conjugate interfaces. Solid and fluid cells are simply treated as part of the same domain with different diffusion coefficients stored at the cell centroids. By calculating the face diffusivity as the harmonic-mean of the values at the centroids sharing the face, the diffusion flux at the conjugate interface is correctly computed (Patankar, 1980).

2.1.4 Staggered Grid

On a staggered grid, the scalar variables (pressure, density, total enthalpy, etc.) are stored in the cell centers of the control volumes, whereas the velocity or momentum variables are located at the cell faces. A staggered storage is mainly used on structured grids for compressible or incompressible flow simulations. Figure 2.3 shows a standard grid used to solve staggered applications.

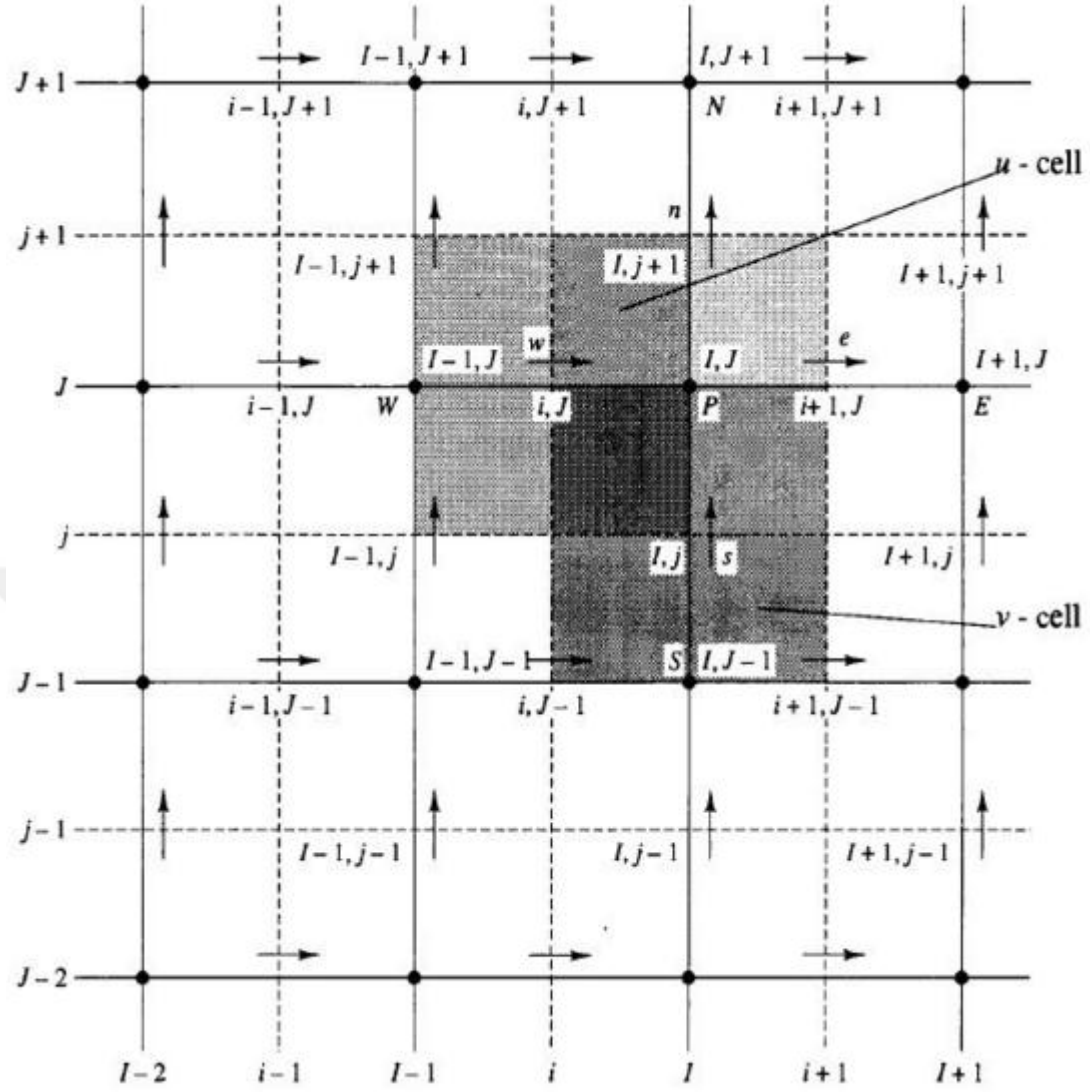

Figure 2.3 Schematic illustration of a staggered grid

The east, west, north and south notations are used to symbolize the vector fields. The *u* component of velocity is stored in the *e* and *w* directions, and the *v* component in the *n* and *s* directions. These are basically vector control volumes different from the scalar pressure control volumes and different from each other. The pressure nodes coincide with the cell faces of the *u*-control volume. The pressure gradient is given by

$$\frac{\partial P}{\partial x} = \frac{P_p - P_W}{\delta x_u} \tag{2.36}$$

$$\frac{\partial P}{\partial y} = \frac{P_p - P_S}{\delta y_v} \tag{2.37}$$

where δx_u is the width of the *u*-control volume, and δy_v is the width of the *v*-control volume.

Using a staggered grid is a simple way to avoid odd-even decoupling between the pressure and velocity. Odd-even decoupling is a discretization error that can occur on collocated grids and which leads to checkerboard patterns in the solutions.

2.1.5 Governing Equations

For incompressible and Newtonian fluids, the time-dependent conservation equations for laminar flow are as follows

Mass:

$$\frac{\partial}{\partial t}(\rho) + \frac{\partial}{\partial x}(\rho u) + \frac{\partial}{\partial y}(\rho v) = 0 \tag{2.38}$$

x-momentum:

$$\frac{\partial}{\partial t}(\rho u) + \frac{\partial}{\partial x}(\rho uu) + \frac{\partial}{\partial y}(\rho vu) = -\frac{\partial p}{\partial x} + \frac{\partial}{\partial x}\left[\frac{\partial}{\partial x}(\mu u)\right] + \frac{\partial}{\partial y}\left[\frac{\partial}{\partial y}(\mu u)\right] \tag{2.39}$$

y-momentum:

$$\frac{\partial}{\partial t}(\rho u) + \frac{\partial}{\partial x}(\rho uv) + \frac{\partial}{\partial y}(\rho vv) = -\frac{\partial p}{\partial y} + \frac{\partial}{\partial x}\left[\frac{\partial}{\partial x}(\mu v)\right] + \frac{\partial}{\partial y}\left[\frac{\partial}{\partial y}(\mu v)\right] - g\left(\rho - \rho_{ref}\right) \tag{2.40}$$

Energy:

$$\frac{\partial}{\partial t}(CT)+\frac{\partial}{\partial x}(CuT)+\frac{\partial}{\partial y}(CvT)=\frac{\partial}{\partial x}\left[\frac{\partial}{\partial x}(kT)\right]+\frac{\partial}{\partial y}\left[\frac{\partial}{\partial y}(kT)\right]-\frac{\partial}{\partial t}(S) \tag{2.41}$$

Equation 2.41 is defined according to the temperature transforming method of Cao & Faghri (1990). This method assumes that phase change occurs between the solidus, $T_{solidus}$ (=$T_m - \delta T_m$), and the liquidus, $T_{liquidus}$ (=$T_m + \delta T_m$) temperatures. C (= ρc) and S terms are temperature dependent properties and can be formulated as

$$C(T)=\begin{cases}(\rho c)_s & T<T_m-\delta T_m\\ (\rho c)_m+\dfrac{h_{sf}}{2\delta T_m} & T_m-\delta T_m\le T\le T_m+\delta T_m\\ (\rho c)_l & T>T_m-\delta T_m\end{cases} \tag{2.42}$$

$$S(T)=\begin{cases}(\rho c)_s(\delta T_m-T_m) & T<T_m-\delta T_m\\ (\rho c)_m(\delta T_m-T_m)+\dfrac{h_{sf}}{2}-\dfrac{h_{sf}}{2\delta T_m}T_m & T_m-\delta T_m\le T\le T_m+\delta T_m\\ (\rho c)_s\delta T_m-(\rho c)_l T_m+h_{sf} & T>T_m-\delta T_m\end{cases} \tag{2.43}$$

$$(\rho c)_m=\frac{(\rho c)_l+(\rho c)_s}{2} \tag{2.44}$$

Except for the specific heat of water (c), thermal conductivity (k) and viscosity (μ) are defined depending on the temperature. Thermo-physical properties of water in solid and liquid phases are given in Table 2.1.

2.1.6 SIS Algorithm

Strongly implicit solver, (Lee, 1989), is used for solving the discretization forms of energy equations. The advantage of using this solver is that the CPU time is reduced a great amount for a single iteration and this solver requires less storage than the other solvers (Ezan, 2006).

Table 2.1 Thermo-physical properties of water and ice (Moraga & Vega, 2004)

Property	Function or Value
c_l (J/kgK)	4204
c_s (J/kgK)	2040
k_l (W/mK)	$-0.63262 + 7.1959\times10^{-3}T - 1.144\times10^{-5}T^2 + 4.2365\times10^{-9}T^3$
k_s (W/mK)	2.2
ρ_l (kg/m^3)	$456.49 + 3.925T - 0.007085T^2$
ρ_s (kg/m^3)	918
μ (Ns/m^2)	$0.038208/(T - 252.33)$

CHAPTER THREE
NATURAL CONVECTION NEAR DENSITY INVERSION

In this research, two types of transient natural convection problems are investigated numerically inside a two-dimensional cavity. One includes a heat transfer of water without phase change (Chapter 3), the other one includes the heat transfer of freezing water (Chapter 4).

3.1 Definition of Problem

The first problem deals with the numerical investigation of transient natural convection of water in a two-dimensional cavity. Water initially remains stagnant ($u = v = 0$), and it has uniform temperature distribution ($T(x, y, 0) = T_C$). It is assumed that top and bottom sides of the cavity are insulated ($dT/dy = 0$), and lateral sides are kept at constant temperature fully or partially ($\xi = H/2$). Figure 3.1 illustrates the case that the lateral surfaces are partially held at T_C and T_H. For all cases, the cold wall assumed to be at $T_C = 0$°C. All parameters that have been used in this problem are given in Table 3.1.

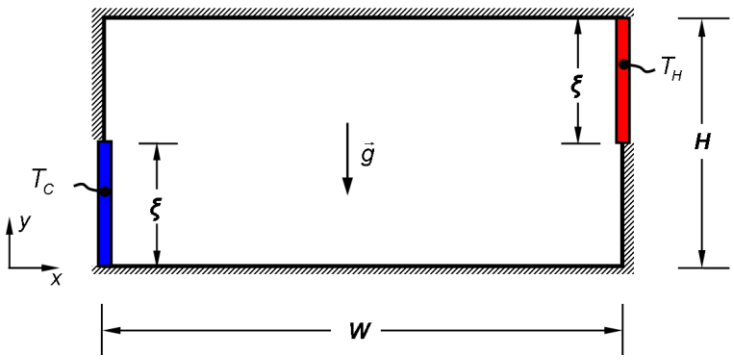

Figure 3.1 Mathematical model

Table 3.1 Numerical Parameters

Case No	ΔT	H/W	ξ
1	4	0.5	H
2		1.0	
3		2.0	
4	8	0.5	H
5		1.0	
6		2.0	
7	16	0.5	H
8		1.0	
9		2.0	
10	8	0.5	
11	8	0.5	
12	8	1	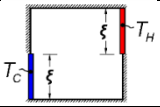
13	8	1	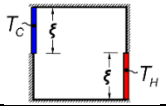

3.2 Validation

The numerical code is generated with control volume approach by using C++ programming language. Power Law scheme (Patankar, 1980) is applied to discretize the convection terms of the governing equations, and SIMPLE algorithm (Patankar, 1980) is implemented to solve the pressure-velocity coupling. Algebraic systems of discretized equations are numerically resolved by using Strongly Implicit Solver of Lee (Lee, 1990). Control volumes are stretched from the walls at a rate of 5% to capture the viscous and thermal boundary layers near the walls of the cavity. Time step size is set as Δt = 0.1 s to be able to catch the time-dependent solutions, and the convergence criteria is defined for each time step as

$$\left|\frac{\phi^{k}-\phi^{k-1}}{\phi^{k}}\right| < 10^{-4} \tag{3.11}$$

A transient natural convection problem that has been studied earlier by experimentally (Banaszek et al., 1999) and numerically (Moraga & Vega, 2004) is

reproduced to prove the accuracy of the current numerical code. In this problem, water is initially stagnant and at 10°C in a square cavity ($H = W = 0.038$ m). One side of the vertical wall is suddenly dropped to 0°C, and the buoyancy-driven convection occurs. Time-dependent flow distribution inside the cavity was obtained experimentally (Banaszek et al., 1999) and numerically (Moraga & Vega, 2004). Figure 3.2 (a, b and c) presents the variations of *y*-component of velocity (v) along the width of the cavity on several vertical positions in comparison with the reference paper (Banaszek et al., 1999). In Figure 3.2(d, e, and f), on the other hand, the variations of *x*-component of velocity (u) through the height of cavity on several horizontal positions are compared with the reference paper (Moraga & Vega, 2004). Consequently, it seems that the velocity distributions that are obtained in the current study are compatible with the experimental data that are measured by Banaszek et al. (1999). On the other hand, Figure 3.2(d, e, and f) reveals that the current predictions have reasonable consistency with the results of the two-dimensional results of Moraga & Vega (2004). However, owing to the influence of three-dimensional flow field and side wall effects, the predicted velocity profiles at $x/H = 0.50$ and $x/H = 0.75$ differ from the results of reference paper for 3D case. The influence of the number of control volumes on the results is also examined. Comparing the predictions for 80x80, 100x100, and 120x120 of control volumes, it seems that 100x100 is an optimum choice. As a result, comparative results suggest that the current code accurately captures the transient natural convection of water in a cavity.

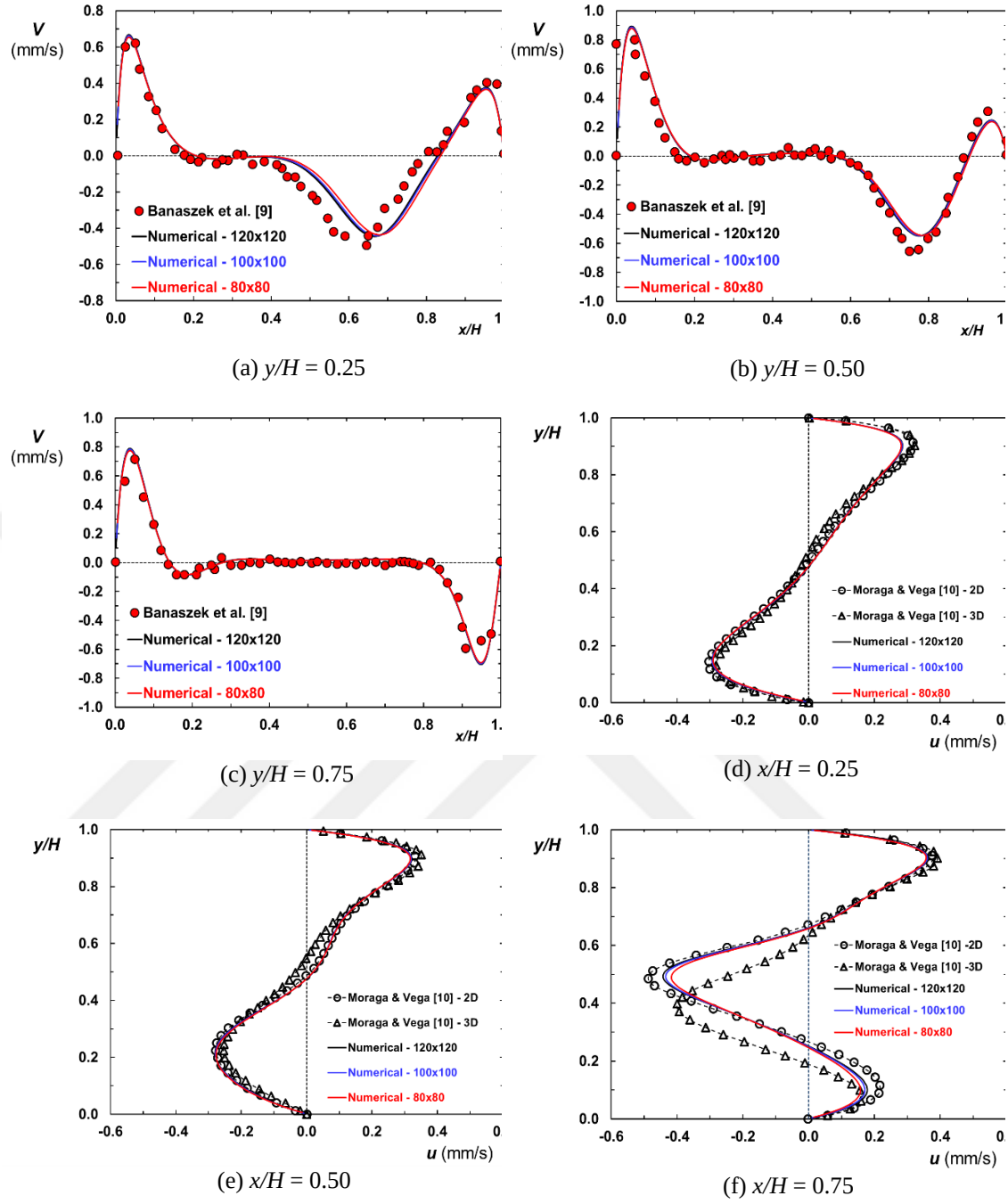

(a) y/H = 0.25 (b) y/H = 0.50

(c) y/H = 0.75 (d) x/H = 0.25

(e) x/H = 0.50 (f) x/H = 0.75

Figure 3.2 Variation of the y and x-components of velocity on position for different planes, t = 2400 s

Figures 3.3 and 3.4 show the isotherms and velocity vectors that are obtained at t = 50 s, 500 s and 1900 s in comparison with the numerical results that are given by Moraga & Vega (2004). Temperature distributions evaluated by this numerical code are similar to the outcome of the reference paper for 2D case. Also, comparison of current velocity vectors and the ones on the reference work show that the size of the secondary circulation cell on the cold wall coincides for t = 500 s and 1900 s.

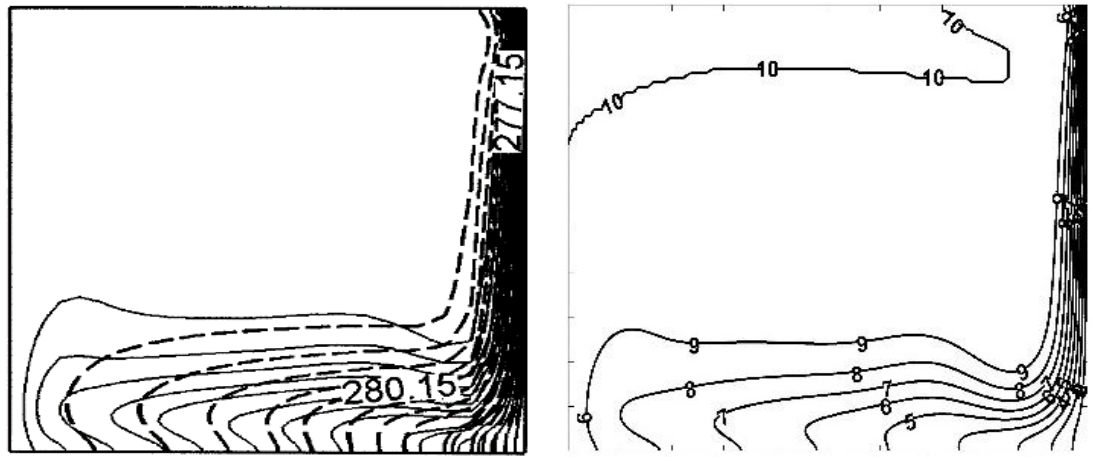

Moraga & Vega (2004) Current

(a)

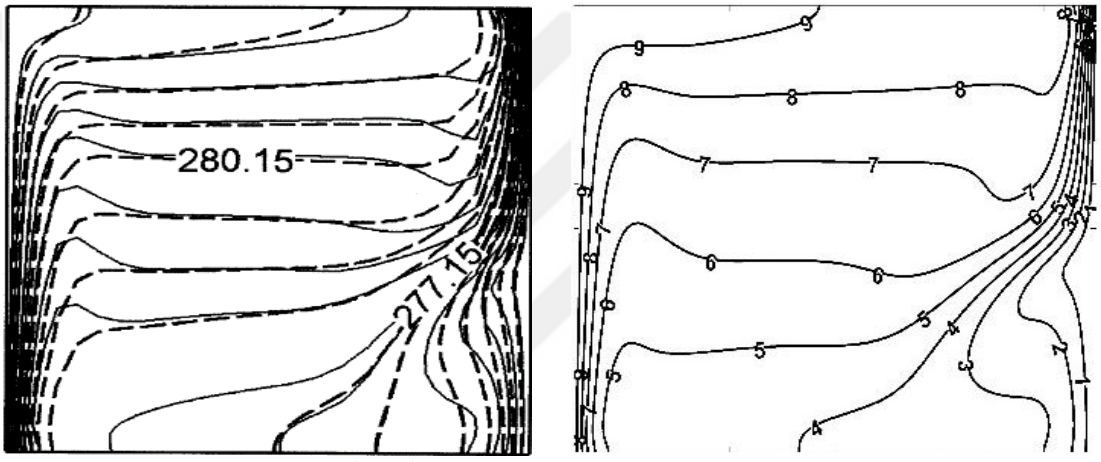

Moraga & Vega (2004) Current

(b)

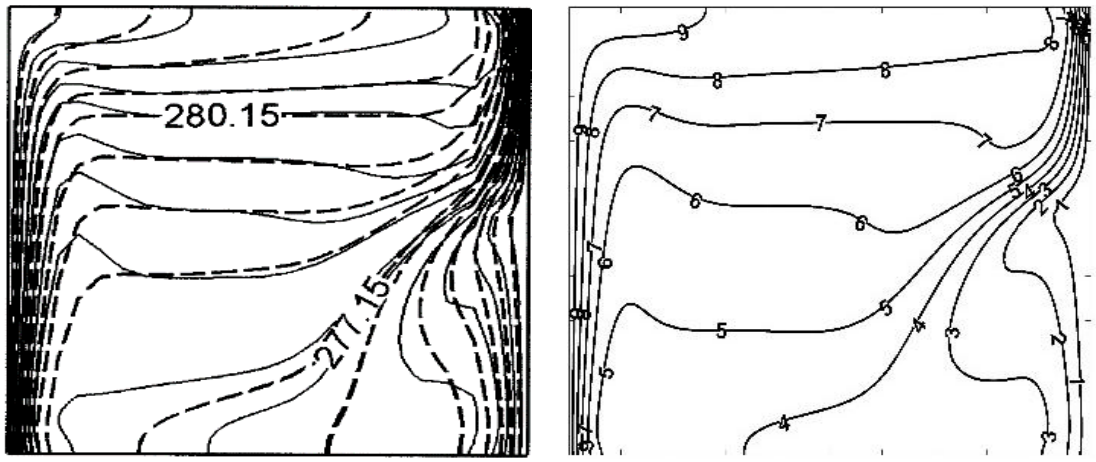

Moraga & Vega (2004) Current

(c)

Figure 3.3 Transient temperature distributions inside the cavity (a) t = 50 s, (b) t = 500 s, (c) t = 1900 s

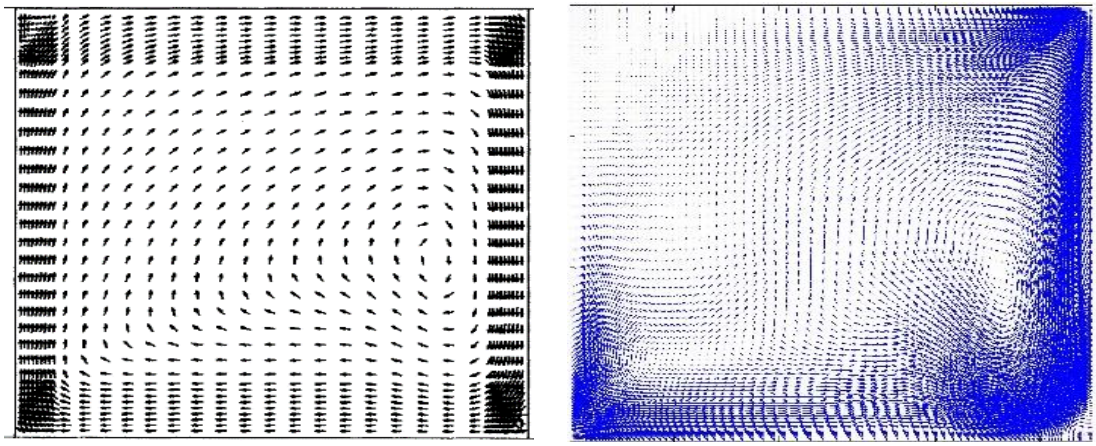

Moraga & Vega (2004) Current

(a)

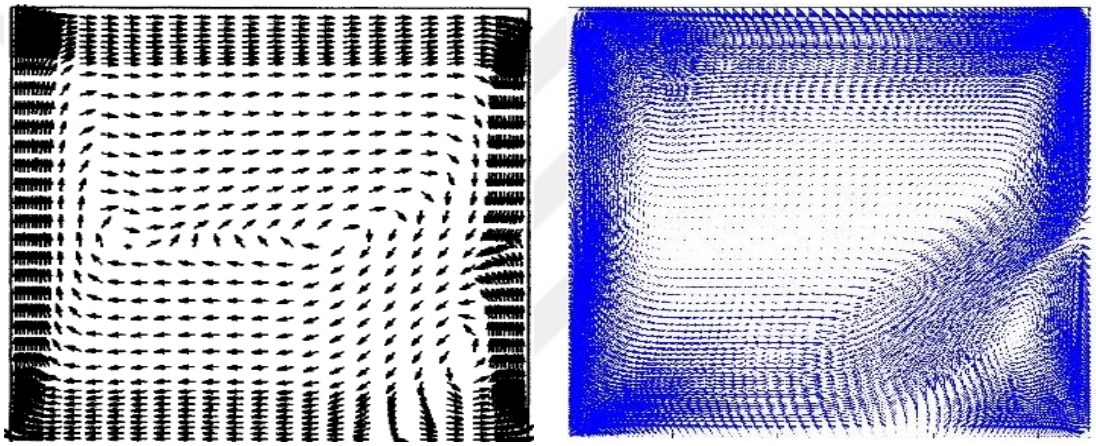

Moraga & Vega (2004) Current

(b)

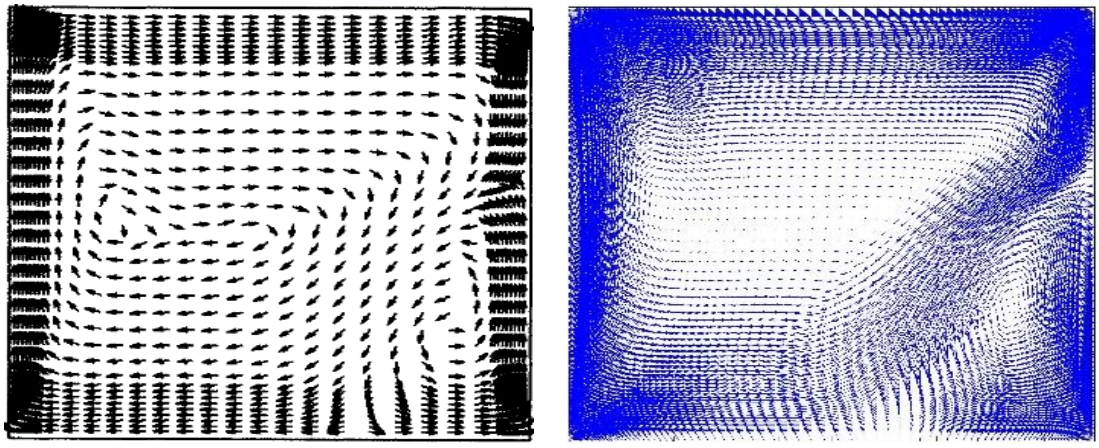

Moraga & Vega (2004) Current Velocity Vectors

(c)

Figure 3.4 Transient velocity distributions inside the cavity (a) t = 50 s, (b) t = 500 s, (c) t = 1900 s

3.3 Results and Discussion

In this section, time-wise Nusselt number variations based on the geometrical and thermal parameters are given at first. After that time-dependent velocity and temperature, distributions are discussed, and local Nusselt variations along the hot wall are obtained.

3.3.1 Average Nusselt Number

Variation of heat transfer rate can be identified regarding the dimensionless Nusselt number. Local Nusselt number over the cold (X = 0) or hot (X = 1) wall is defined by using dimensionless parameters as,

$$\mathrm{Nu} = \left|\frac{\partial\theta}{\partial X}\right|_{X=0,1} \tag{3.2}$$

where, θ $(=(T-T_C)/(T_H-T_C))$ is the dimensionless temperature and X (=x/H) represents the dimensionless position. To obtain the area-weighted average Nusselt number on a surface, following definition is used,

$$\overline{\mathrm{Nu}} = \frac{1}{A}\int_0^A \left|\frac{\partial\theta}{\partial X}\right|_{X=0,1} dY \tag{3.3}$$

where, Y (= y/H) corresponds to the dimensionless vertical position.

Figure 3.5(a) shows the time-wise variation of the average Nusselt number on the cold wall. For R = 1.0 (Case 1, 2, and 3), Nusselt number exponentially increases independently from the aspect ratio. It seems that Nusselt numbers do not significantly change after t = 1500 s, which means that the problems approach the steady-state. On the other hand, for R = 0.5 (Case 4, 5, and 6), step-like changes are observed in the time-wise variations of Nusselt numbers. After a certain flow-time, a secondary circulation cell forms on the hot wall, and that may cause those alterations. For all three cases, it takes 4500 s to let the liquid reaches a steady-state condition. For R = 0.25 (Case 7, 8, and 9) sudden increments are obtained on the time-wise

variation of Nusselt number after t = 300 s. Since the temperature difference is higher, secondary circulation cells forms on the hot wall in the early stages and grows up through the cold wall rapidly. It seems that it takes 2500 s to reach a steady-state condition. For partially active heating/cooling walls, (Case 10 to 13), it is clear that the aspect ratio slightly affects the Nusselt number. For Case 11 and 13, in which the heating part is placed on the upper half of the wall, a significant difference between the Nusselt numbers is observed at the initial periods. Nusselt numbers approach to each other with increasing time and become identical when the flow is reached a steady-state condition. For Case 10 and 12, the heating part is placed in the lower half of the wall. It seems that there is no significant difference between the surface Nusselt numbers. Figure 3.5(b) shows the variation of the average Nusselt number as a function of density inversion parameter (R) and aspect ratio (*H/W*) at the steady-state condition. For R = 0.25, the temperature difference between side walls are maximum (T_h = 16°C), so the Nusselt numbers have also higher values. For R = 0.5, although the hot wall temperature is T_h = 8°C, the Nusselt number is lower than the one that is obtained at R = 1.0 (T_h = 4°C). Basically, for R = 0.5, two separate circulation cells occur inside the cavity, and the increasing friction loss inversely affects the convective heat transfer.

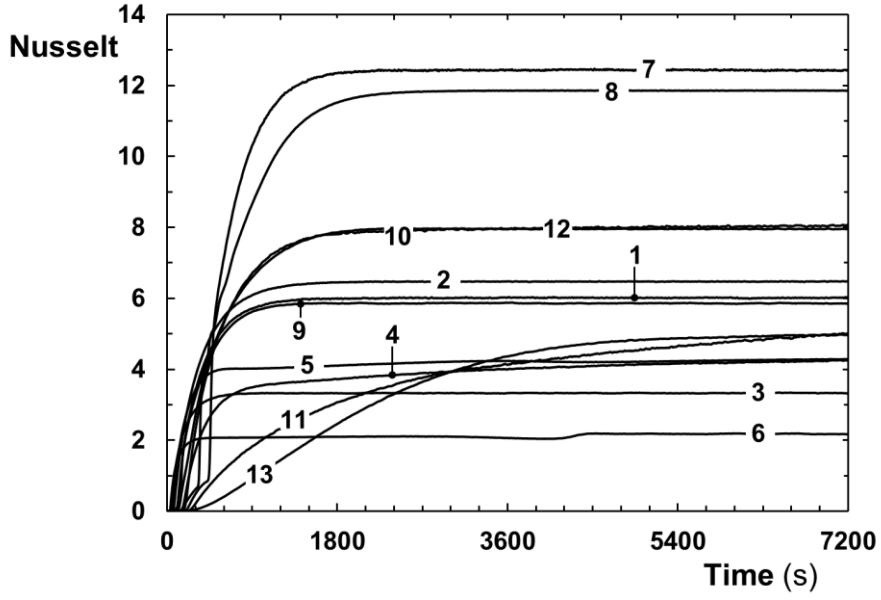

(a)

Figure 3.5 Nusselt number variations (a) Time-wise variation, (b) steady-state

Figure 3.5 continues

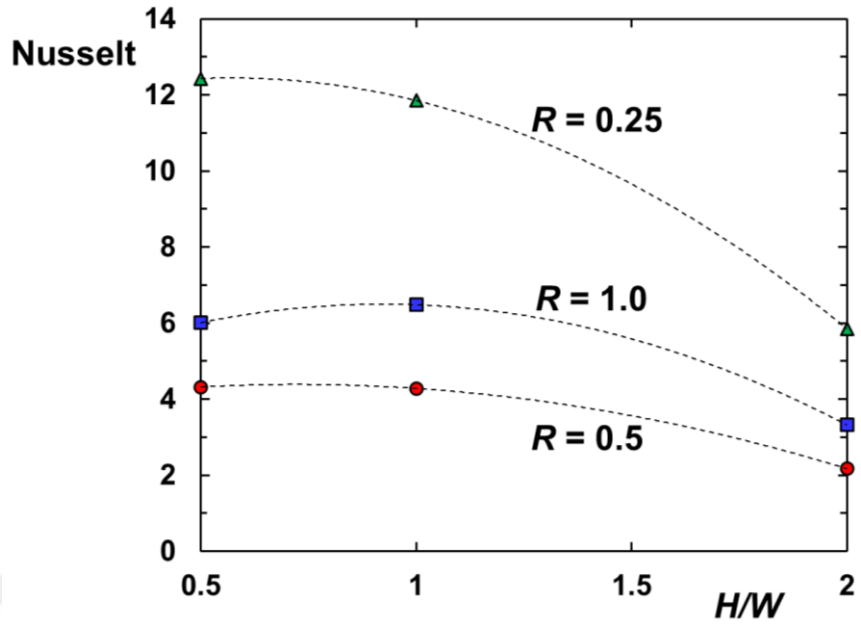

(b)

3.3.2 Velocity and Temperature Fields

In Figure 3.6, isotherms and streamlines are given for the aspect ratio of (H/W) = 1.0 and R = 0.5. At t = 300 s, a secondary circulation cell appears near the bottom side of the hot wall. There are two circulation zones in the cavity that are separated by the density inversion temperature of water (T_m = 4°C). For $T > T_m$, density decreases with increasing the temperature, so that, there is a counter-clockwise circulation zone near the hot wall. On the other hand, a clockwise circulation cell is dominant for the region that is below the T_m. At t = 900 s, the secondary circulation cell grows in the vertical direction and covers the hot wall. t = 7200 s, on the other hand, represents the steady-state condition. According to the previous findings in the literature (Lin & Nansteel, 1987; Wei & Koster, 1994), for the case of R = 0.5, under the steady-state condition and with constant thermo-physical properties, the density inversion temperature (T_m) divides the cavity by two equal parts. Current predictions, on the other hand, reveals that the circulation cell on the right-hand side of the cavity is bigger than the cold one, and the symmetry of the isotherms (or streamlines) deteriorate. Unlike from the common approach in literature (Lin & Nansteel, 1987; Wei & Koster, 1994), this study takes into account temperature dependent viscosity and thermal conductivity of water. It is a well-known fact that the viscosity of water

decreases with increasing the temperature. So, that, the circulation cell on the right-hand side of the cavity may grow more easily owing to the lower viscosity values. For R = 0.5, the effect of friction reduces the buoyancy forces on the density inversion plane, thus the rate of heat transfer also decreases. Even though the temperature difference of R = 0.5 (ΔT = 8°C) is bigger than R = 1.0 (ΔT = 4°C), friction losses decrease the heat transfer rate or the surface Nusselt number.

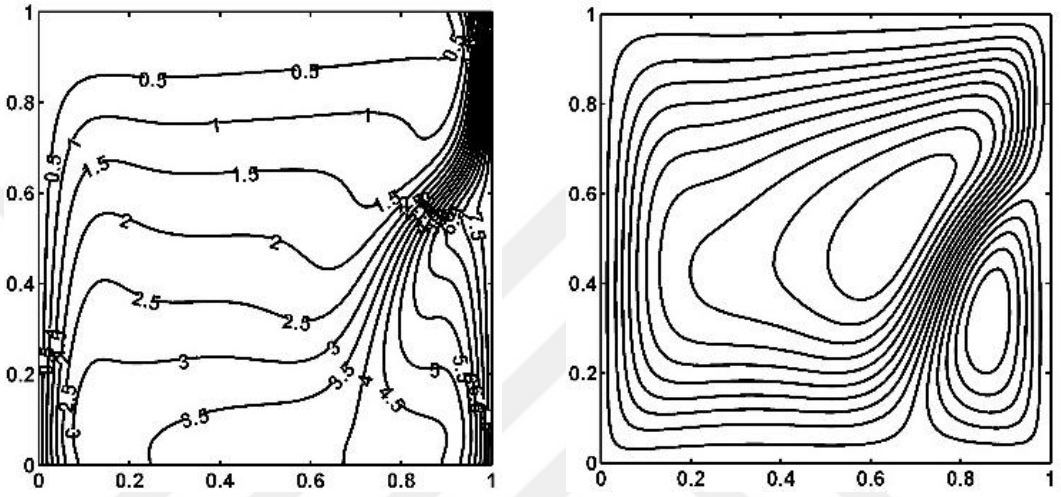

(a)

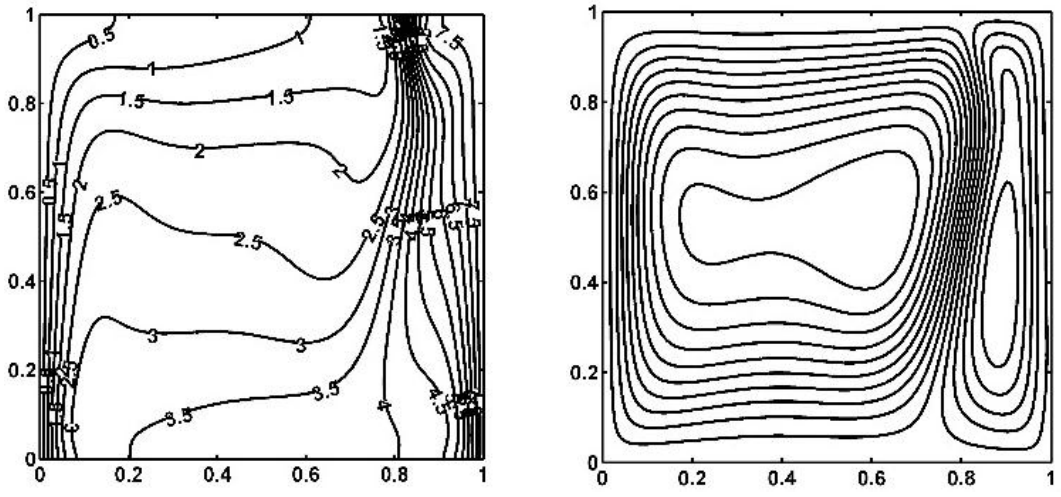

(b)

Figure 3.6 Isotherms (left) and streamlines (right) for Case 5 (H/W) = 1.0, R = 0.5 (a) t = 300 s, (b) t = 900 s, (c) t = 7200 s

Figure 3.6 continues

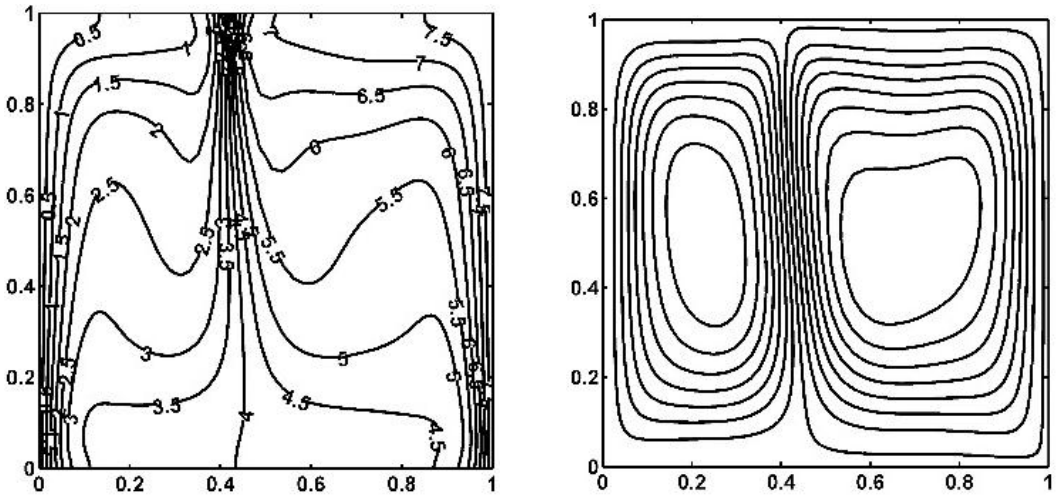

(c)

Figure 3.7 shows the isotherms and streamlines at t = 300 s, 900 s and 7200 s for (H/W) = 2.0 and R = 0.5. Since the cavity height is taller than the one in Case 5, the buoyancy forces become more efficient in this geometry. At t = 300 s, the secondary circulation cell almost covers the hot wall and influential over the half of the cavity width. In the advancing time, counter-clockwise circulation cell grows through the cold wall and suppresses the clock-wise cell at the steady-state condition. Results reveal in the tall cavities that, unlike the square case, there is no symmetry between circulation cells for R = 0.5.

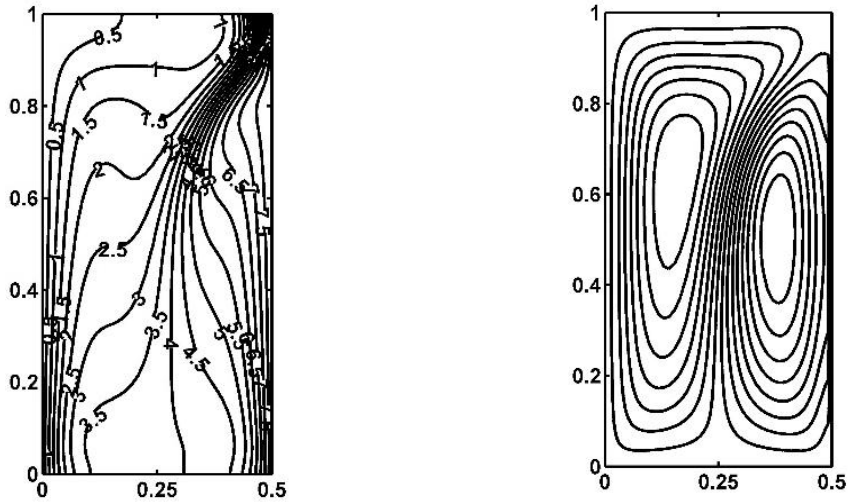

(a)

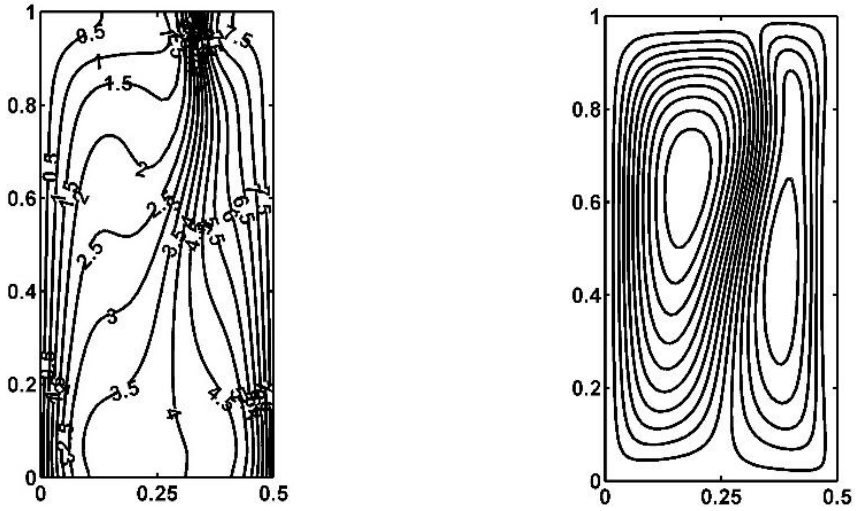

(b)

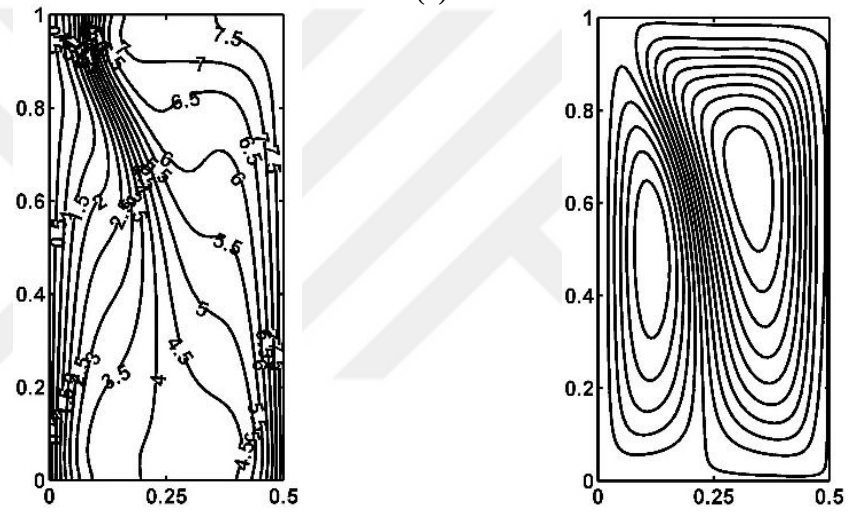

(c)

Figure 3.7 Isotherms (left) and streamlines (right) for Case 6 (H/W) = 2.0, R = 0.5 (a) t = 300 s, (b) t = 900 s, (c) t = 7200 s

Figure 3.8 indicates the natural convection characteristics in a cavity with an aspect ratio of (*H/W*) = 0.5 and *R* = 0.5. In the current geometry, the generation of secondary circulation cell near the hot wall resembles the one in the square cavity (Case 5). At *t* = 300 s, counter-clockwise circulation cell appears at the bottom side of the hot wall and grows along the vertical direction on the later on. At the steady-state condition, there are two asymmetric circulation cells and the counter-clockwise circulation cell shifts the other one to the cold wall and dominates almost 60% of the cavity width.

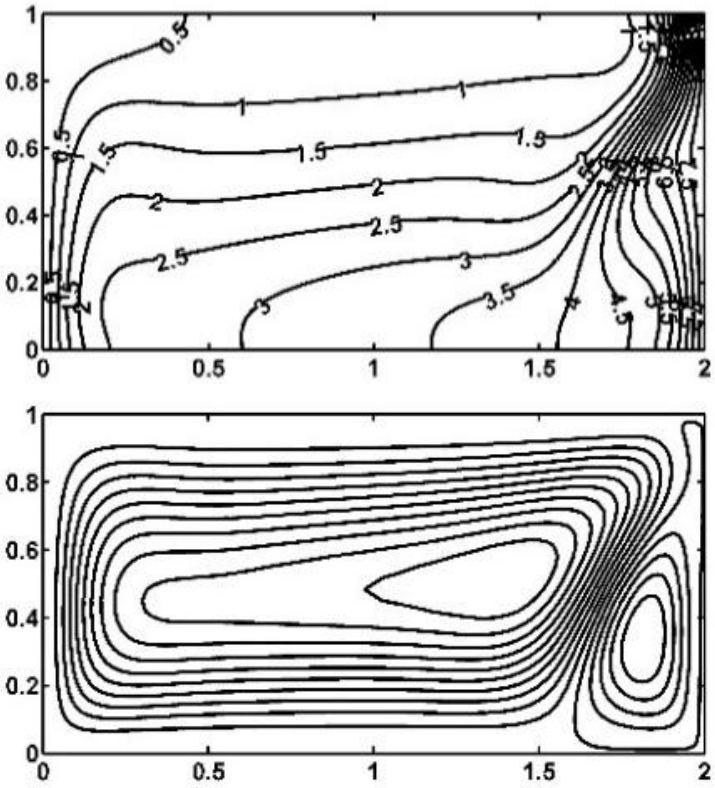

(a)

Figure 3.8 Isotherms (top) and streamlines (bottom) for Case 4, (H/W) = 0.5, R = 0.5 (a) t = 300 s, (b) t = 900 s, (c) t = 7200 s

Figure 3.8 continues

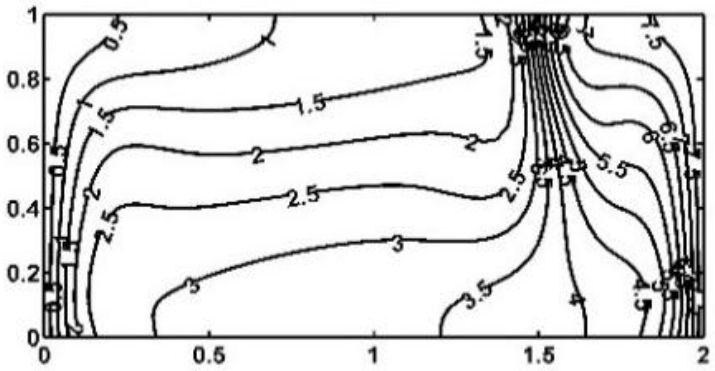

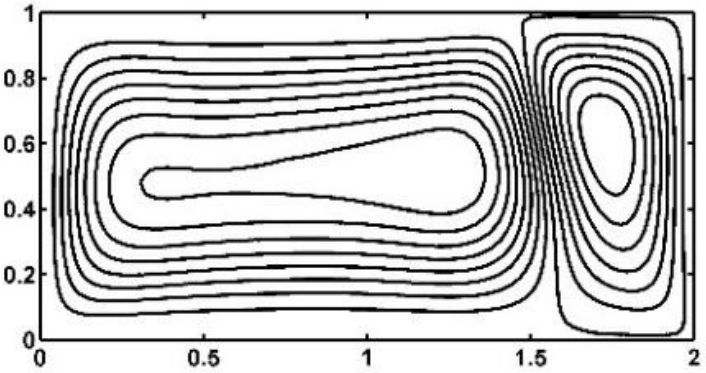

(b)

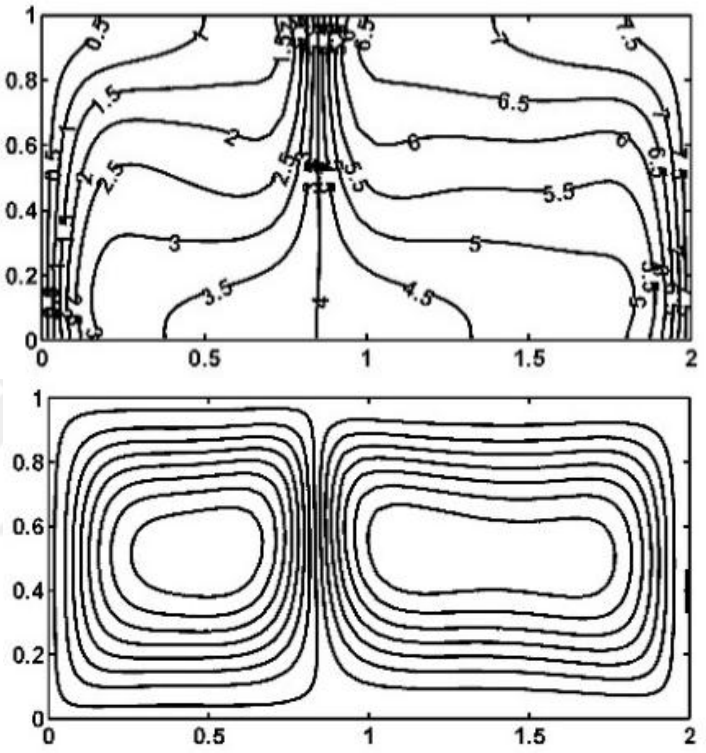

(c)

In the remaining part of the problem, short (H/W = 0.5) and square (H/W = 1.0) cavities are reconsidered with partially active walls. As given in Table 3.1, partially active hot and cold walls are simulated for each geometry. Figure 3.9 represents the generation of natural convection for Case 10. While the upper half of the right wall is hot, the lower half of the left wall is cold. In comparison with the full active wall cases, the formation of secondary circulation zone is delayed. A small counter-clockwise cell is observed at t = 900 s on the top-right corner of the cavity. The cell grows diagonally and at the steady-state condition, it can only be effective near a small place close to the active hot wall. Figure 3.9 gives the variation of the local Nusselt number at different flow times. The arrow that seems in this figure represents

the increasing time. At the beginning of the process, the temperature gradients on the hot wall are higher, so that Nusselt number has maximum values at initial times. In ascending time, temperature gradients decrease at the top of the cavity so that local Nusselt number is also reduced. Since the temperature gradients are higher at the leading edge of the hot wall after t = 900 s, the sudden increment on the Nusselt number along the vertical direction becomes more remarkable in Figure 3.10.

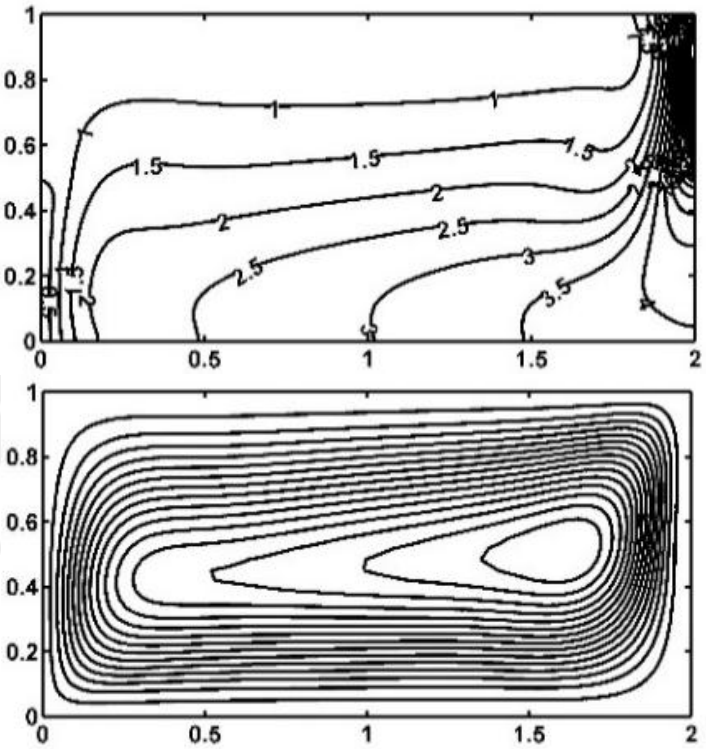

(a)

Figure 3.9 Isotherms (left) and streamlines (right) for Case 10, (H/W) = 0.5, R = 0.5 (a) t = 300 s, (b) t = 900 s, (c) t = 7200 s

Figure 3.9 continues

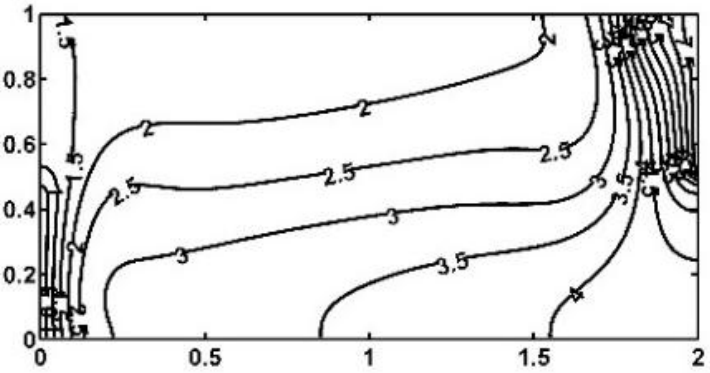

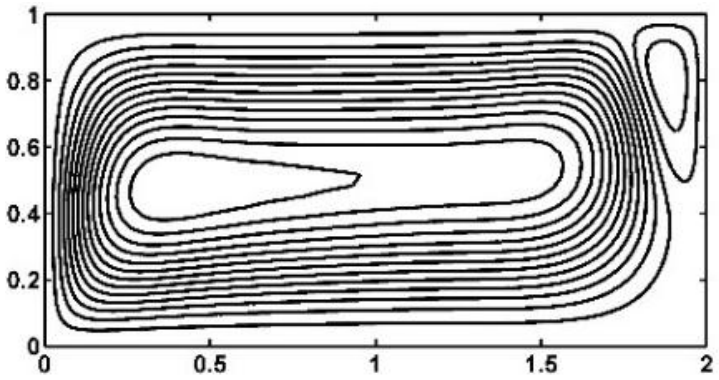

(b)

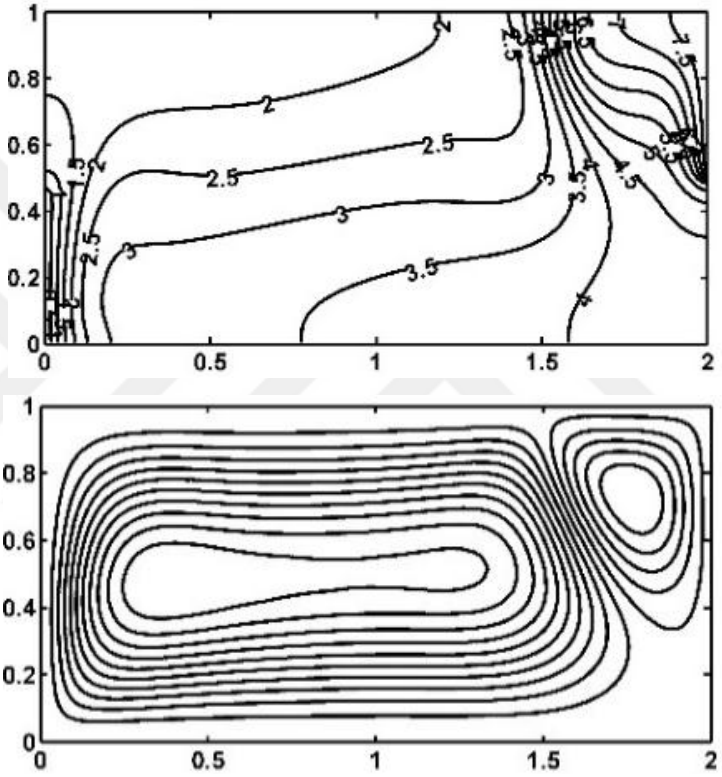

(c)

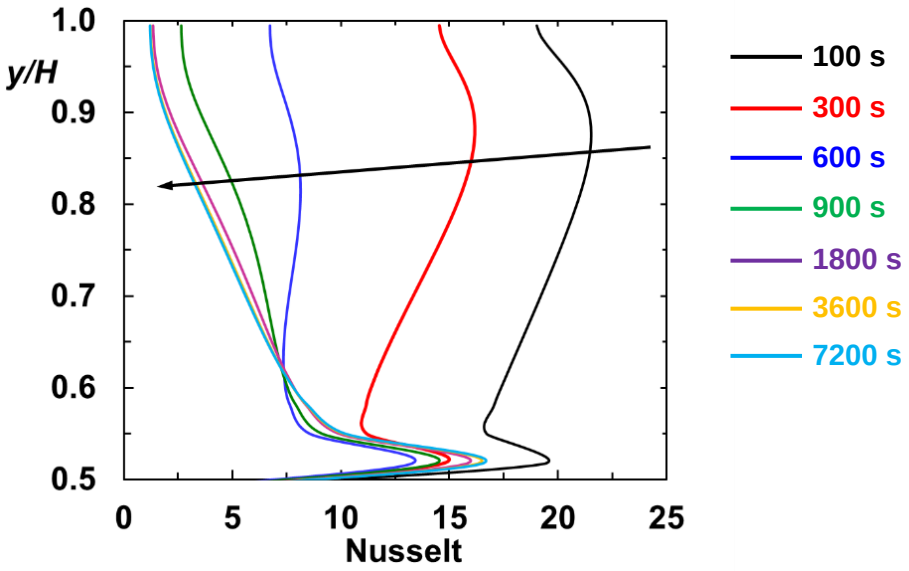

Figure 3.10 Time-wise variation of local Nusselt number on hot wall for Case 10, (H/W) = 0.5, R = 0.5

Figure 3.11 reveals the formation of natural convection for Case 11. The lower half of the right wall is hot, and the upper half of the left wall is cold. The growing rate of secondary circulation cell is higher than the one in Case 10. At steady-state condition, counter-clockwise circulation cell dominates the whole domain, but the clockwise circulation cell becomes active only near the cold wall at the top-left corner of the cavity. As seen in Figure 3.12, because of the higher heat transfer rates on the hot wall, Nusselt number has greater values, especially at the initial periods with respect to Case 10. The thermal plume that is obtained at the initial periods (t = 300 s and 900 s) induces the higher gradients on top of the hot wall so that the Nusselt number values become enormous.

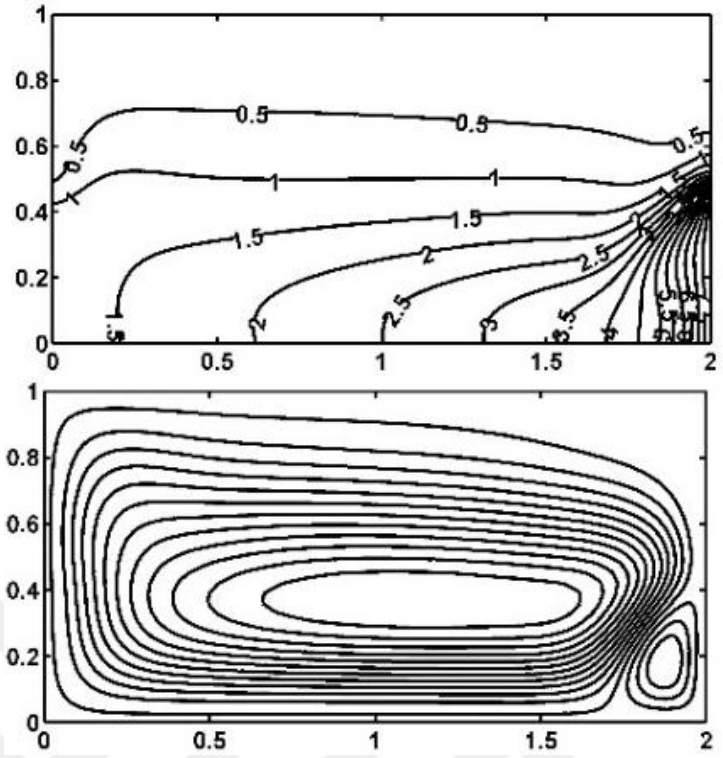

(a)

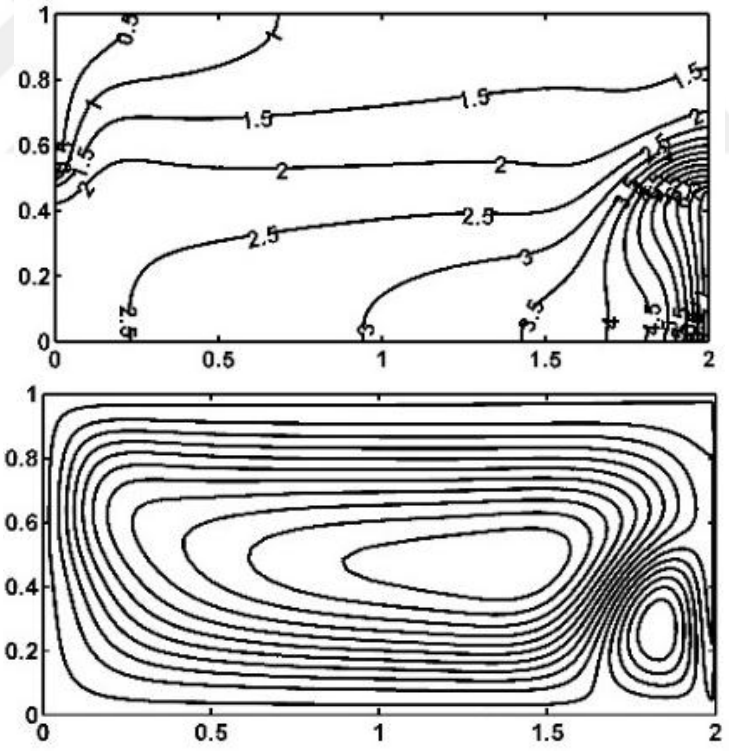

(b)

Figure 3.11 Isotherms (left) and streamlines (right) for Case 11, (H/W) = 0.5, R = 0.5 (a) t = 300 s, (b) t = 900 s, (c) t = 7200 s

Figure 3.11 continues

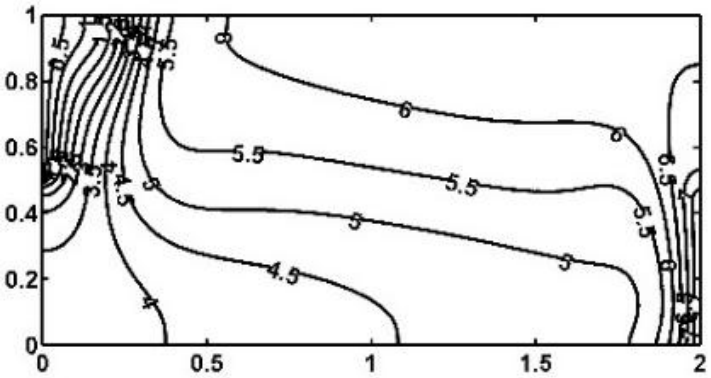

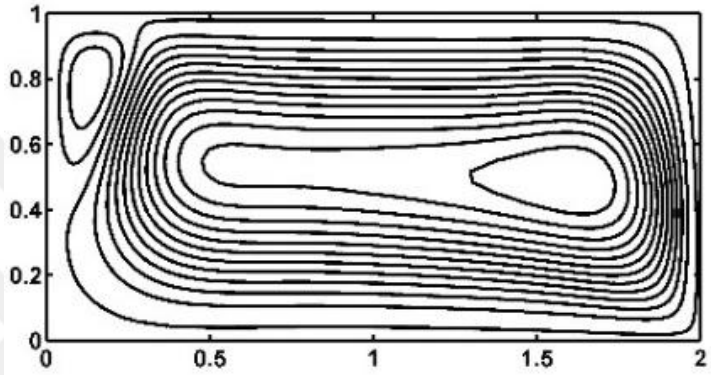

(c)

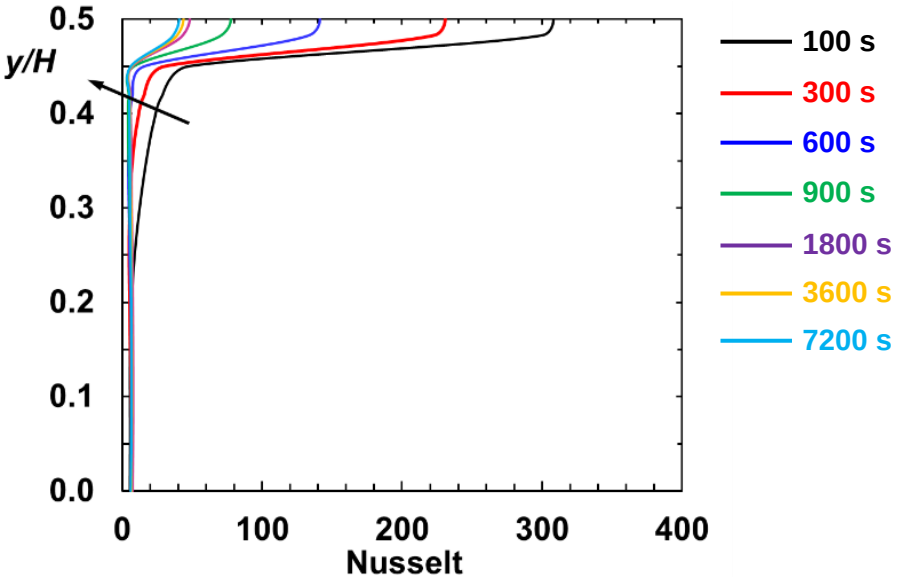

Figure 3.12 Time-wise variation of local Nusselt number on hot wall for Case 11, (H/W) = 0.5, R = 0.5

Figure 3.13 indicates the time-wise variation of natural convection for the partially heated/cooled square cavity for Case 12. The upper half of the right wall is

hot, and the lower half of the left wall is cold. Single clockwise circulation is dominant for this problem. The center of circulation cell moves from the hot wall through the middle of the cavity and extends. A weak counter-clockwise cell is observed at the steady-state condition. The variation of the local Nusselt number at selected flow times are given in Figure 3.14. The space-wise variations have the similar tendencies, but the magnitudes decrease in time. After t = 600 s, variations of Nusselt number are altered owing to the formation of the secondary circulation near the hot wall. Relatively higher values are also observed close to the lower half of the hot wall.

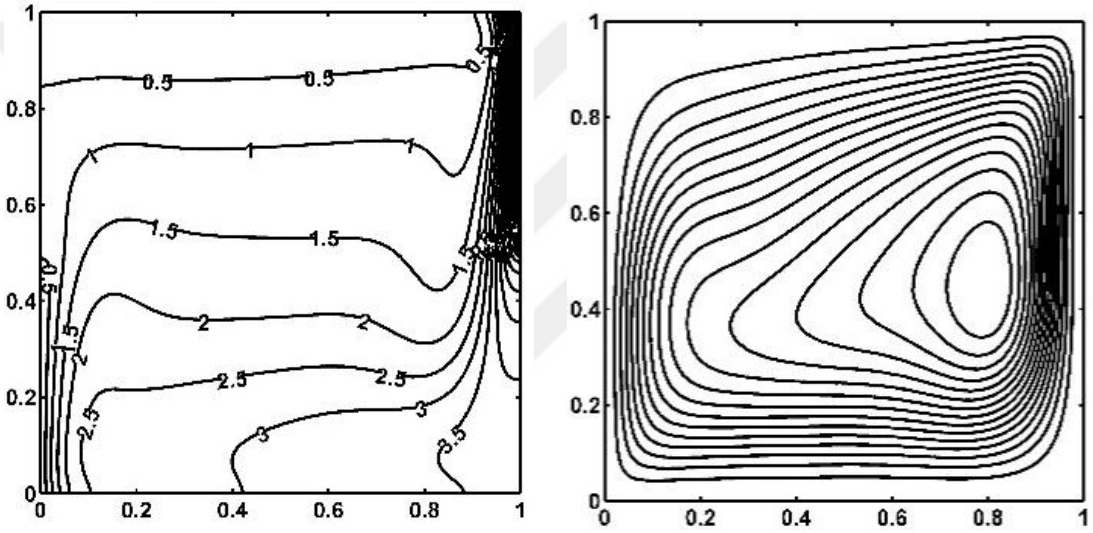

(a)

Figure 3.13 Isotherms (left) and streamlines (right) for Case 12, (H/W) = 1.0, R = 0.5 a) t = 300 s, b) t = 900 s, c) t = 7200 s

Figure 3.13 continues

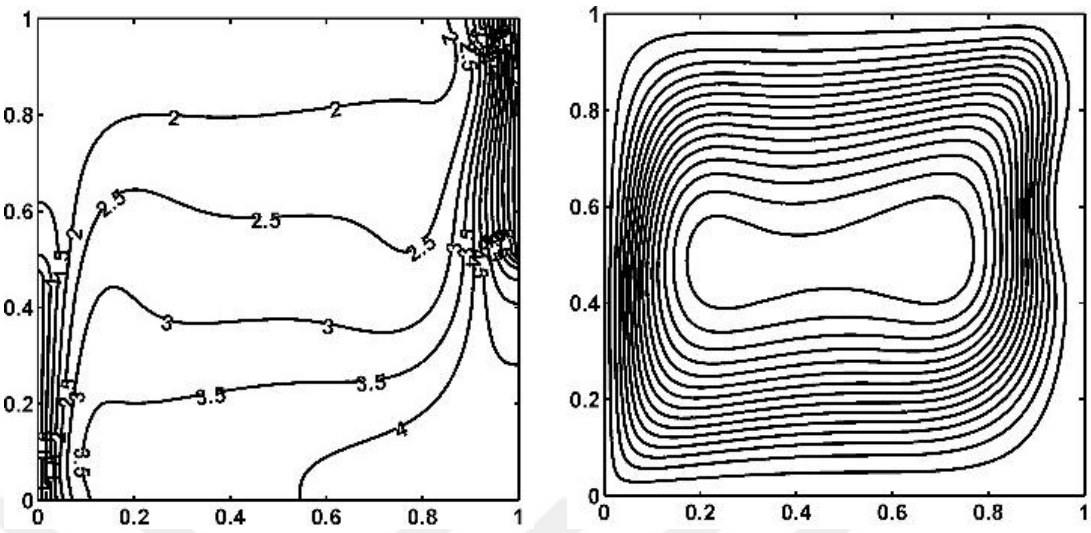

(b)

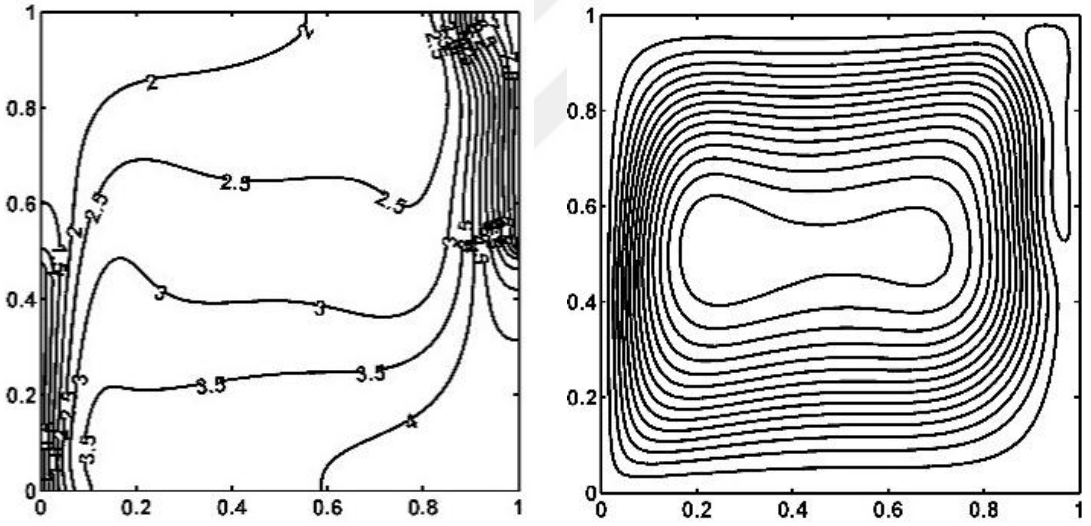

(c)

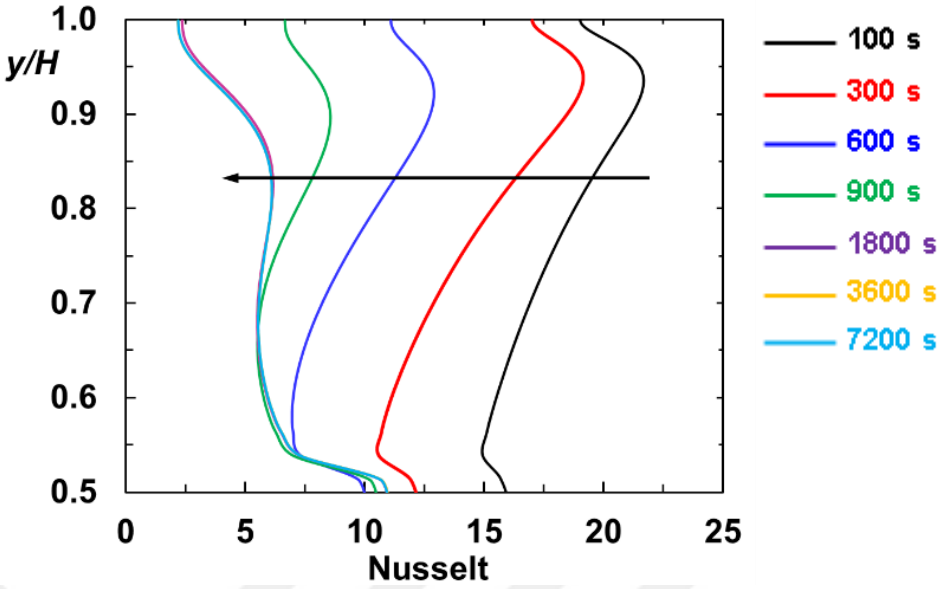

Figure 3.14 Time-wise variation of local Nusselt number on hot wall for *Case* 12, (*H/W)* = 1.0, *R* = 0.5

In Figure 3.15 and 3.16, isotherms, streamlines, and local Nusselt number variations are represented for Case 13. While the lower half of the right wall is hot, the upper half of the left wall is cold. Similar to the Case 11, a thermal plume is observed near the partially active hot wall at the initial periods. A secondary anti-clockwise circulation cell can be seen at t = 300 s. In time, the secondary circulation grows and dominates into the cavity. The steady state streamlines and isotherms look similar to the ones that are obtained in Case 12. It should be kept in mind that the circulation is the clockwise rotation for Case 12, on the other hand, the circulation is the counter-clockwise rotation for Case 13. Local Nusselt number variations also look alike with the Case 12. It is obvious that Case 12 reaches the steady-state condition faster than Case 13.

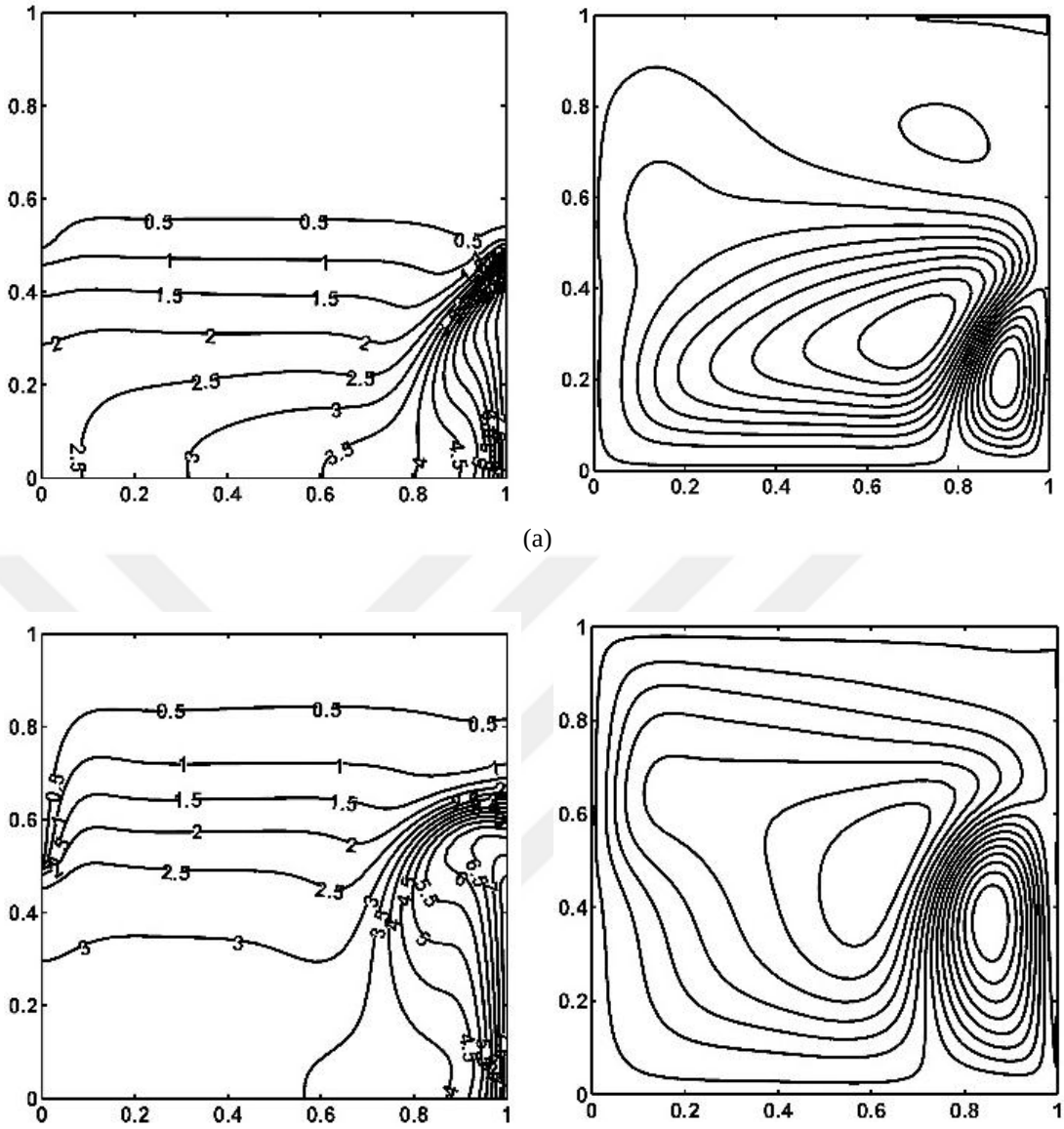

Figure 3.15 Isotherms (left) and streamlines (right) for Case 13, (H/W) = 1.0, R = 0.5 (a) t = 300 s, (b) t = 900 s, (c) t = 7200 s

Figure 3.15 continues

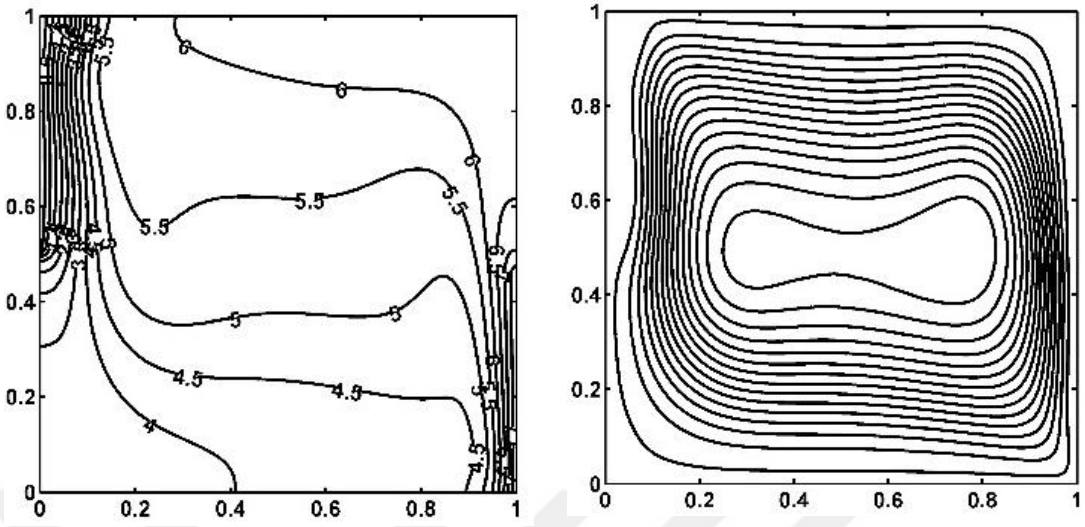

(c)

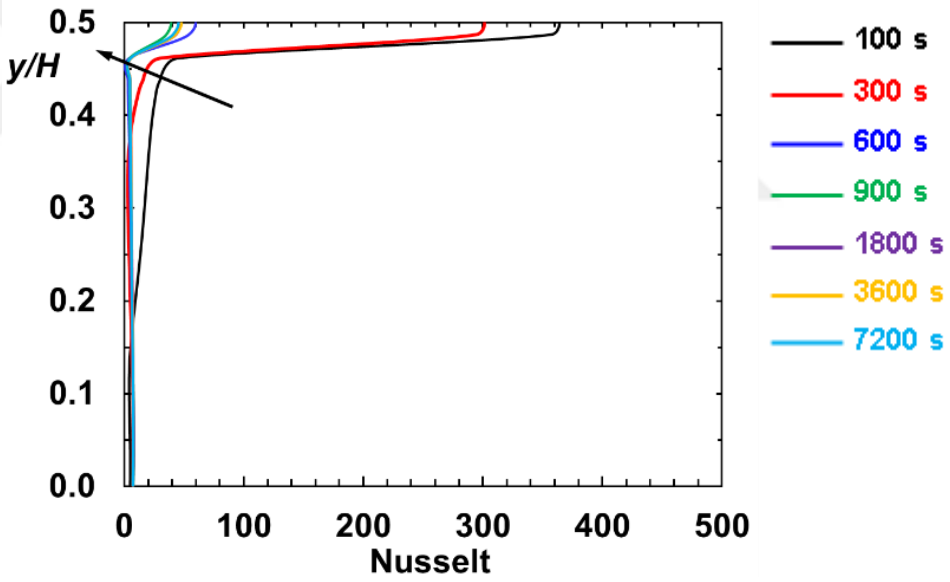

Figure 3.16 Time-wise variation of local Nusselt number on hot wall for Case 13, (H/W) = 1.0, R = 0.5

CHAPTER FOUR
NATURAL CONVECTION DRIVEN PHASE CHANGE NEAR DENSITY INVERSION

4.1 Definition of Problem

This problem involves the numerical investigation of transient natural convection of freezing water in a two-dimensional square cavity (H = W = 0.038 m). Water initially remains stagnant (u = v = 0), and it has uniform temperature distribution (T_{in} (x, y, t = 0) = T_∞). It is assumed that the walls are made of Plexiglas with 5 mm thickness. There is a heat gain from the surrounding fluid flow through the system from the selected three walls. The external fluid is at T_∞ with a convective heat transfer coefficient of h. The remaining wall, which is made of Plexiglas (k = 0.2 W/mK) with the same thickness as others, is maintained at a predefined temperature that is below the freezing temperature of water. As seen in Figure 4.1, three different cold wall positions are considered to examine the effect of the direction of the solidification on the heat transfer. In order to visualize the effect of convection and conduction during solidification of water, heat transfer coefficient (h_{wall}), and the thermal conductivity of the wall (k_{wall}) are varied, respectively. Overall heat transfer coefficient of the cold wall (U_{wall}) is also defined to combine the effects of convection and conduction terms in one parameter. Figure 4.1 illustrates the boundary conditions and the cooling scenarios that are considered in this problem. Whole parameters that have been used in this problem are also given in Table 4.1.

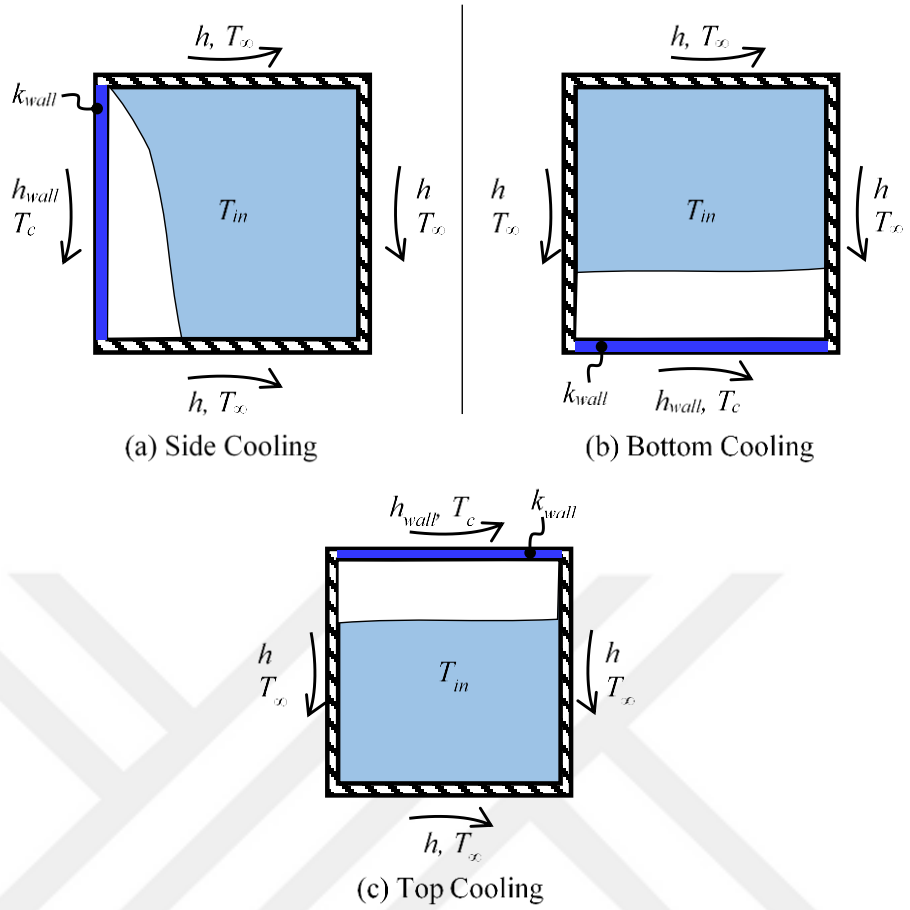

Figure 4.1 Schematic illustrations of the situations

Table 4.1 Numerical parameters

T_{in}	10°C
T_{∞}	10°C
h	20 W/m^{2}K
k	0.2 W/mK
T_c	-10°C
h_{wall}	10 ~ 1000 W/m^{2}K
k_{wall}	0.5 ~ 100 W/mK
H/W	1

4.2 Validation

The numerical code is generated with control volume approach in C++ programming language. Power Law scheme (Patankar, 1980) is applied to discretize the convection terms of the governing equations, and CUT (Consistent Update Technique) algorithm (Jin, Tao, He, & Li, 2008) is implemented to solve the

pressure-velocity coupling. This algorithm converges faster than SIMPLE family of algorithms, and it reduces CPU time by at least 15–63% with much better robustness when solving melting/freezing problems (Wang, Faghri, & Bergman, 2010). Algebraic systems of discretized equations are numerically resolved by using Strongly Implicit Solver of Lee (1989). Control volumes are stretched from the walls at a rate of 5% to capture the viscous and thermal boundary layers near the walls of the cavity. Time step-size is set as $\Delta t = 0.1$ s to be able to catch the time-dependent solutions, and the convergence criteria is defined for each time step as in the Equation (3.1).

A transient natural convection of freezing of water, which has already been studied experimentally by Banaszek et al. (1999), is reproduced to prove the accuracy of our numerical code. In this problem, water is initially stagnant and is at 10°C in a square cavity ($H = W = 0.038$ m). The sudden change of temperature of the lateral cold wall from 10°C to −10°C causes an ice formation on this cold wall and shifts two competing vortices toward the hot lateral wall. Experimental results of the conjugate heat transfer problem (combination of the heat transfer in both in insulation and water) inside the cavity gives the flow structure that is similar to our numerical results. Figures 4.2 and 4.3 represent the variations of *y*-component of velocity (v) along the width of the cavity on several vertical positions at $t = 500$ s and $t = 3000$ s, respectively, in comparison with the reference paper (Banaszek et al., 1999).

In figures, the solid circles, filled with red color, are the experimental data of the reference work. The dashed lines with rectangular (Case 1) and triangular (Case 2) symbols represent the numerical results of the reference paper without and with heat gain from the remaining walls, respectively. It is clear that the predictions for Case 2, in which heat gain from the top, bottom and sidewall is considered, has better consistency with the experimental data. The dashed (blue) and straight (red) lines, on the other hand, are the current predictions for the cases without and with heat gain, respectively. It seems that the velocity distributions that are obtained in our study, especially for the case in which heat gain is taken into account, are compatible

with the experimental data of Banaszek et al. (1999). As a result, comparative results suggest that current code accurately captures the transient natural convection of freezing of water in a square cavity.

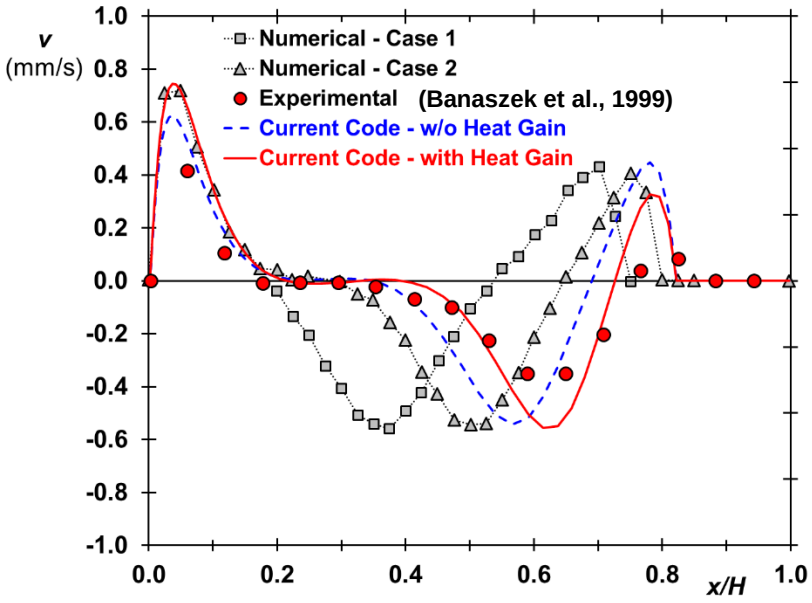

(a)

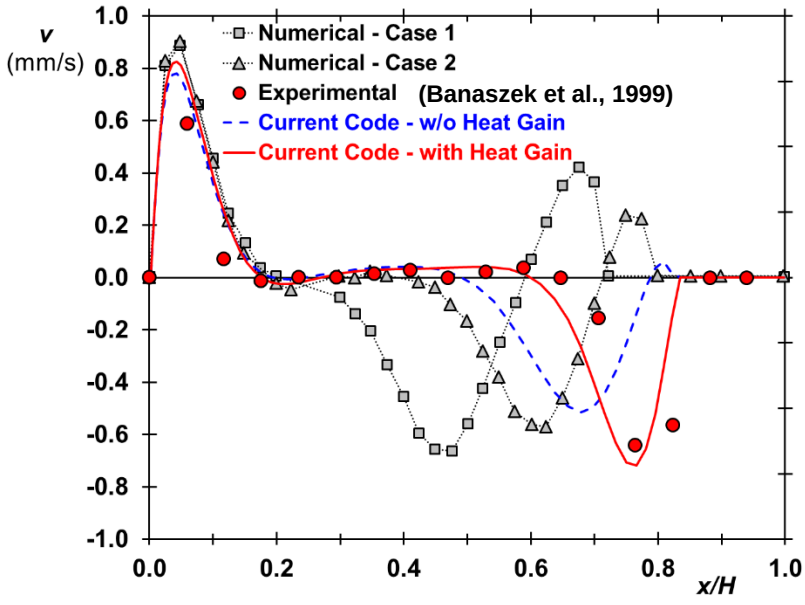

(b)

Figure 4.2 Variation of the y-component of velocity on position on different planes at t = 500s (a) y/H = 0.25, (b) y/H = 0.50, (c) y/H = 0.75

Figure 4.2 continues

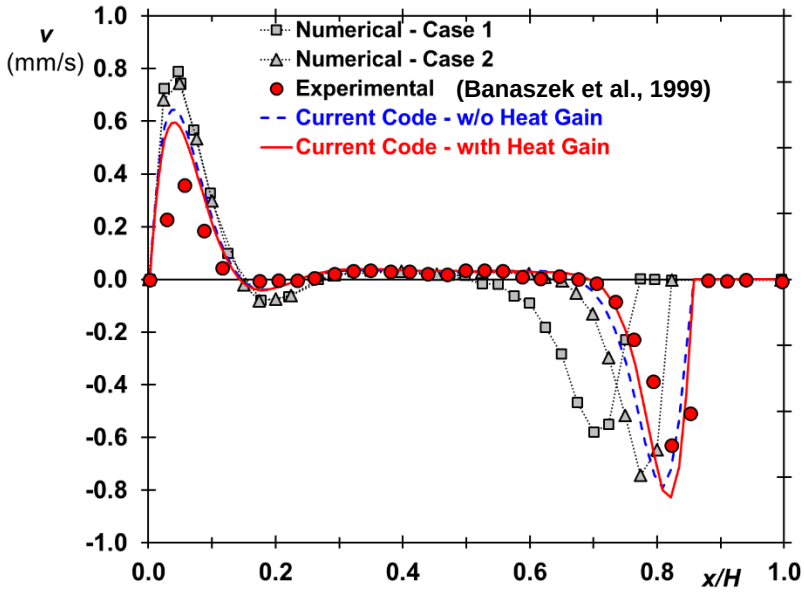

(c)

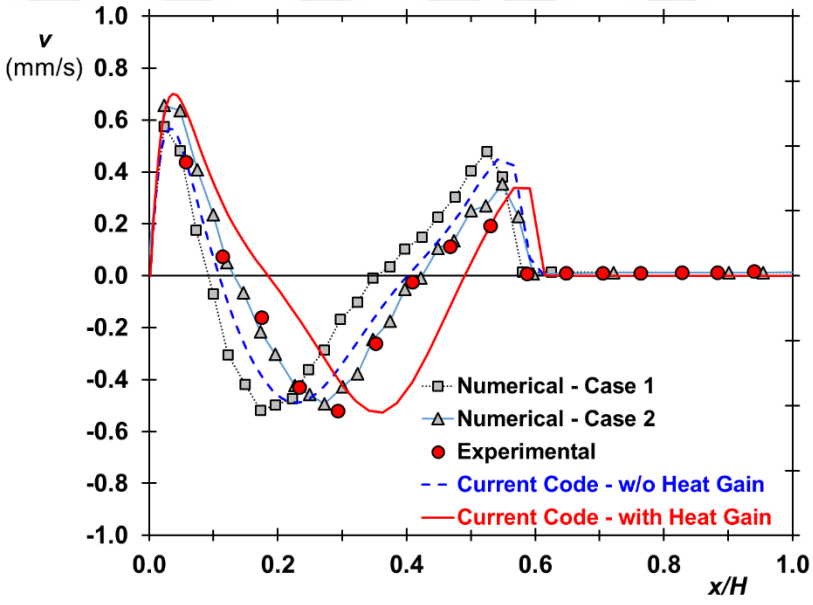

(a)

Figure 4.3 Variation of the y-component of velocity on position on different planes at t = 3000s (a) y/H = 0.25, (b) y/H = 0.50, (c) y/H = 0.75

Figure 4.3 continues

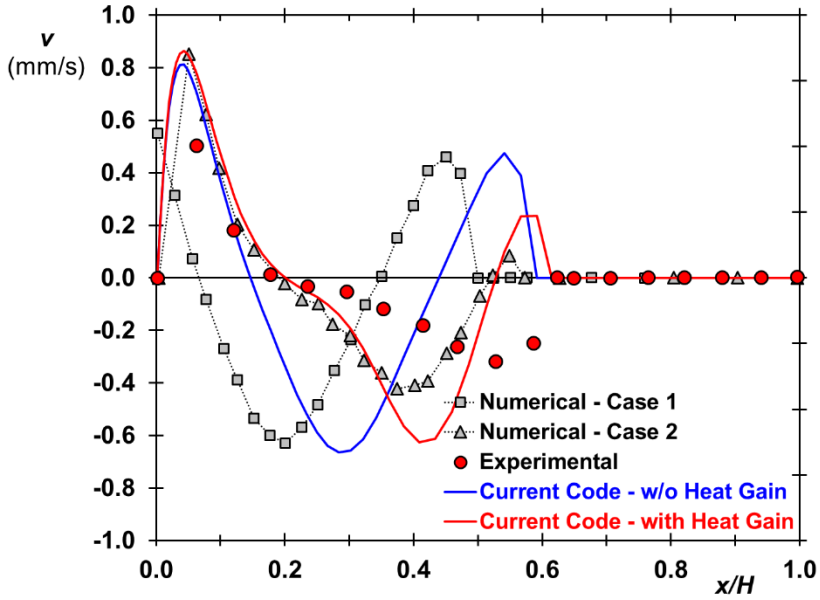

(b)

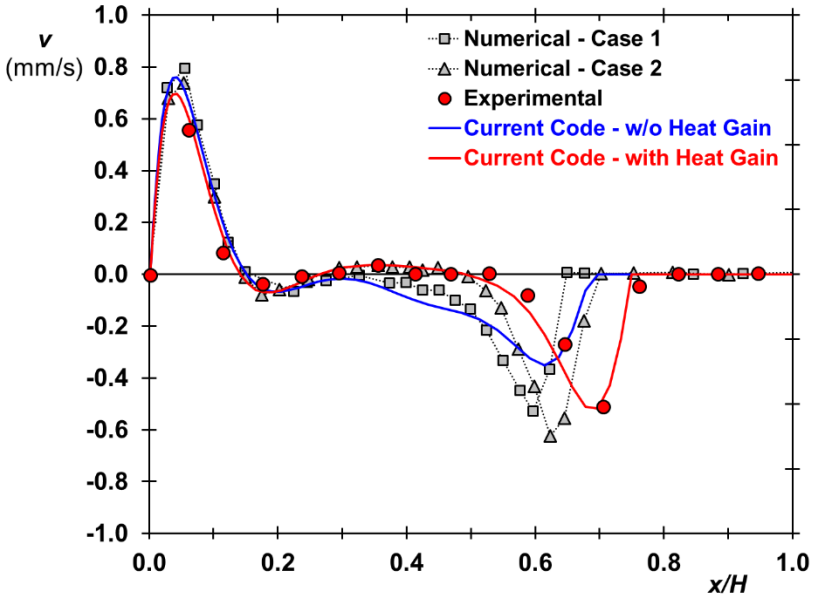

(c)

4.3 Results and Discussion

4.3.1 Side Cooling

Time-wise variations of side wall temperature as a function of overall heat transfer coefficient (U) are given in Figures 4.4 and 4.5. Convective heat transfer coefficient on the side wall is changed from 10 to 5000 W/m^{2}K, and thermal conductivity of the side wall material is defined in the range of 0.5 and 100 W/mK. Overall heat transfer coefficient is given in figures to compare the combined effects of convective and conductive resistances. Increasing the overall heat transfer coefficient of the cold wall enhances the cooling rate of water. For U > 83.3 W/m^{2}K, the side wall temperature drops below 0°C within 360 s. Besides, for U < 20 W/m^{2}K, the cooling rate considerably reduces. The effect of density inversion of water (4°C) becomes clear at lower cooling rates. When the side wall temperature goes down below 4°C, the wall temperature suddenly decreases and then tends to increase. The formation of clockwise circulation cell near the cold wall may cause this abnormal variation. It is also clear that the difference between conduction and convection dominated phase change processes becomes significant at lower U values, which corresponds lower cooling rates. Figure 4b and 5b reveal that the difference between conduction and convection becomes remarkable when the side wall temperature is higher than the phase change temperature of water (0°C).

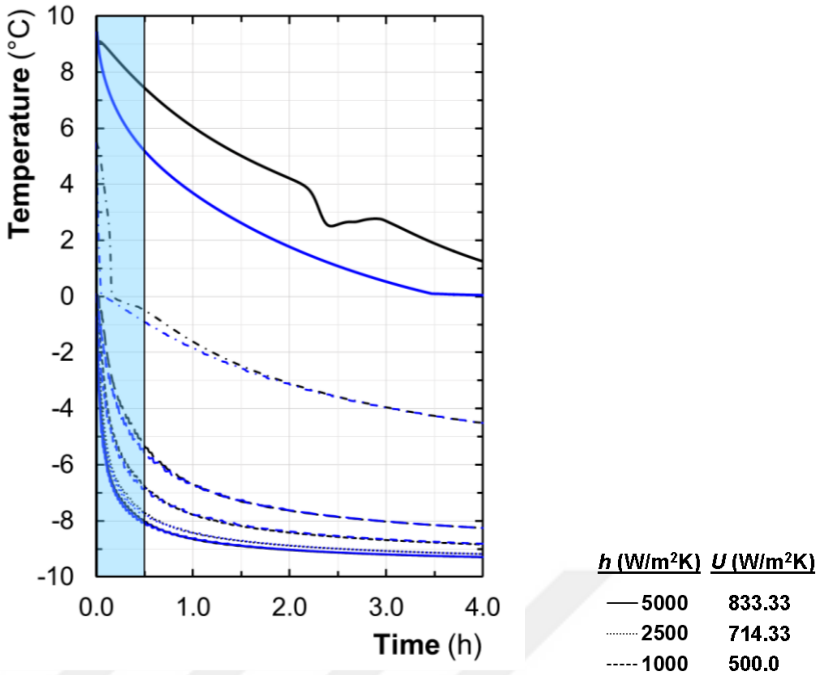

(a)

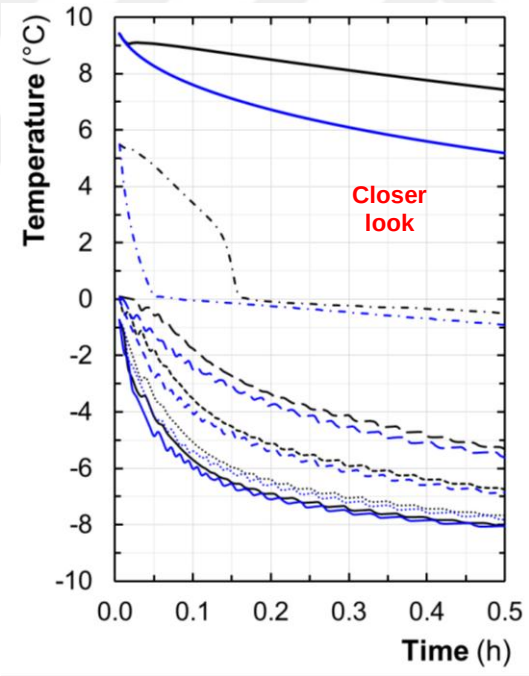

(b)

Figure 4.4 a) Effect of convective heat transfer coefficient on wall temperature Side Cooling Without (blue) and with (black) natural convection b) closer look

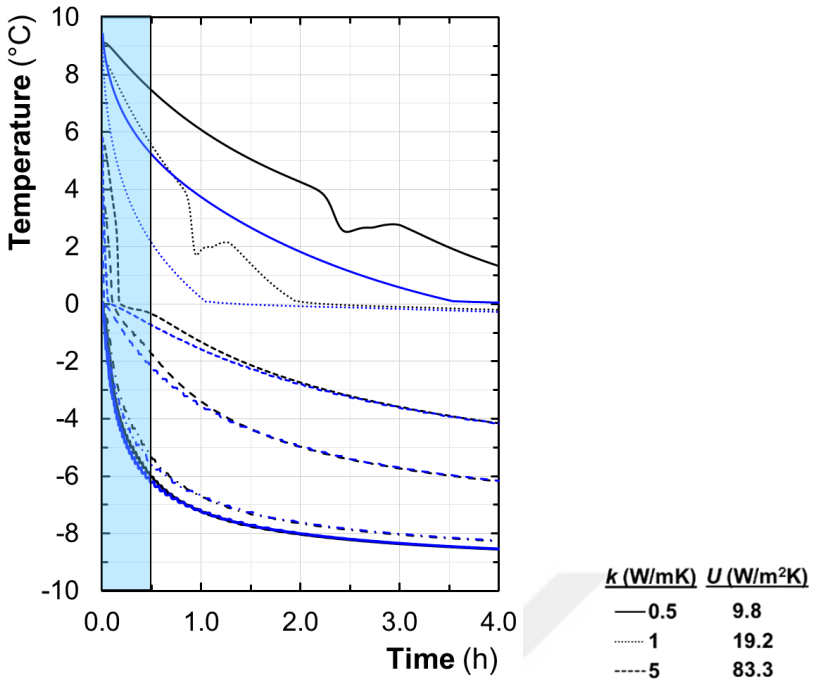

(a)

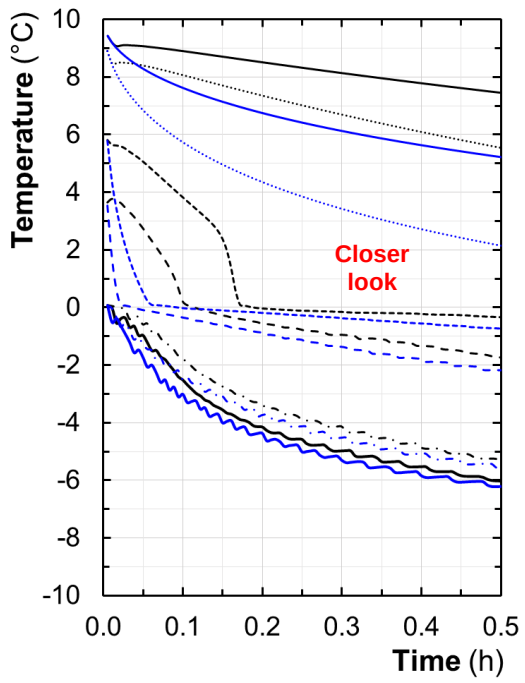

(b)

Figure 4.5 a) Effect of thermal conductivity on wall temperature Side Cooling Without (blue) and with (black) natural convection b) closer look

It is interesting to note that the lowest wall temperatures are observed for the conduction dominated heat transfer condition. To explain this phenomenon, temperature contours are compared in Figure 4.6 at U = 833.33 W/m^{2}K. As seen in Figure 4.6(a), isotherms are almost vertical for conduction dominated case. Lines distort near the walls owing to the heat gain from the warmer surroundings. On the contrary, isotherms are being disordered for convection dominated case, as given in Figure 4.6(b). Domain is separated into two parts around the density inversion line of water (4°C), the clockwise and counter-clockwise circulation cells are generated on the right and left-hand side of the density inversion line, respectively. Anti-clockwise circulation cell brings hot water through the cold side. That is, the temperature gradients become larger on the upper-left of the domain. The higher temperature gradients mean that the convective heat transfer on the ice is more effective near the top wall. The high heat transfer rate on the upper-left restrain the ice growth, and the shape of the ice is distorted. Ice grows through the diagonal direction. From bottom to top the thickness of the ice reduces almost by half. It should be noted that the average temperature of water reduces quite faster for the convection dominated phase change. Circulation cells let the cold water penetrates into the domain more easily. Since the hot current blocks the ice growth on the cold wall for the convection dominated phase change, the average temperature of the cold wall decreases quite faster in the conduction dominated case.

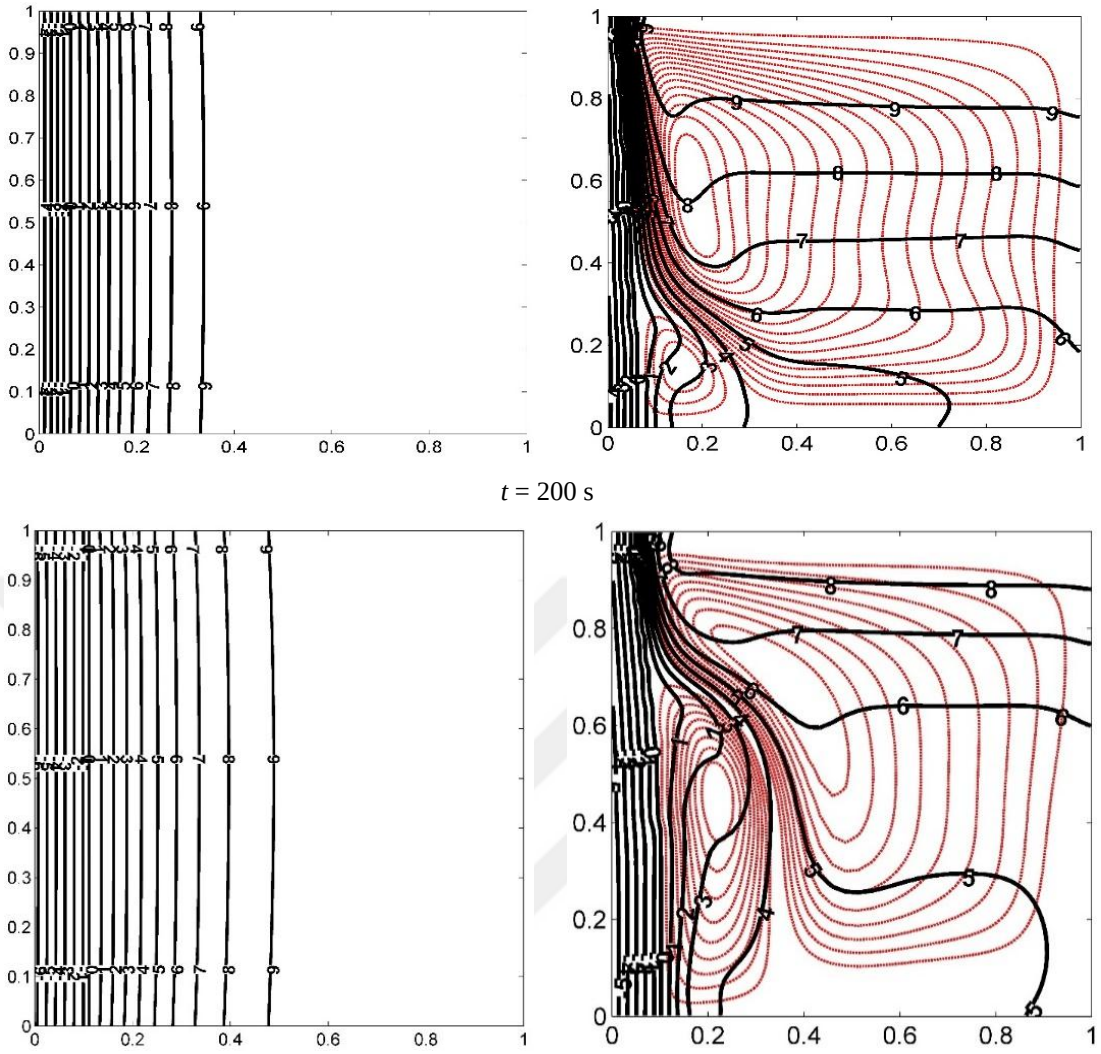

Figure 4.6 Temperature contours for a) Conduction and b) Convection dominated phase change, Side Cooling, U = 833.33 W/m^{2}K

In Figures 4.7 and 4.8, the thermal energy storage capability of the conduction and convection dominated cases are compared using dimensionless effectiveness. This is defined as a ratio of the change in enthalpy to the maximum possible enthalpy change,

$$\varepsilon(t) = \frac{H(t) - H(t=0)}{\Delta H_{\max}} \tag{4.1}$$

It can be seen that the influence of convection becomes significant for the initial period of this process ($0 < t < 0.5$ h). Owing to the formation of natural convection during phase change process, the ability of energy storage, effectiveness, is slightly higher for convection dominated case, especially $t < 0.5$ h. The effectiveness is nearly 10% greater than the one in conduction dominated case for $U = 833.3$ W/m^{2}K. Results also reveal that the effect of overall heat transfer coefficient on the effectiveness is more remarkable for relatively lower U values. The impact of overall heat transfer coefficient diminishes with increasing the U values. For instance, increasing U from 9.90 to 90.91 W/m^{2}K, the effectiveness increases nearly 5.5 times. On the other hand, the difference between U = 333.33 and 833.33 is nearly 10% regarding the effectiveness.

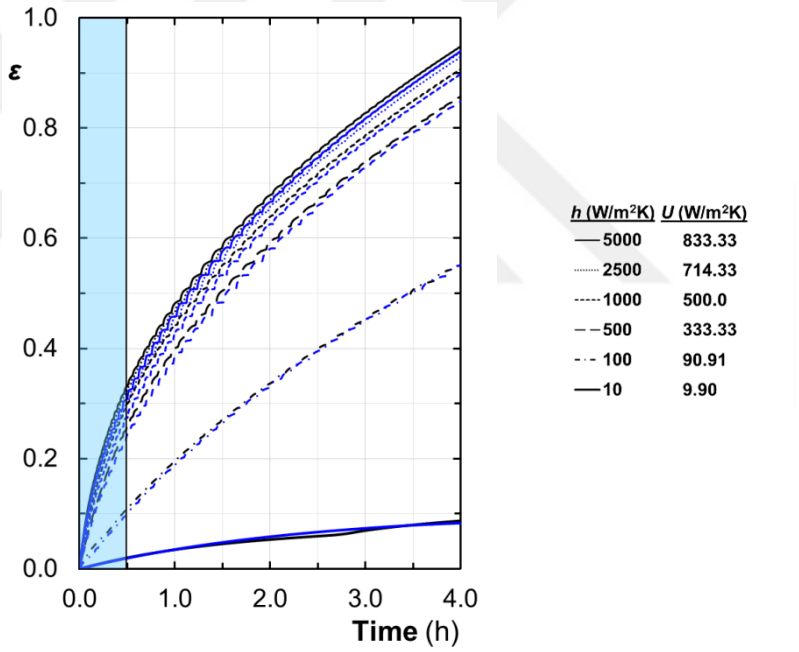

(a)

Figure 4.7 a) Effect of convective heat transfer coefficient on effectiveness, Side Cooling Without (blue) and with (black) natural convection b) closer look

Figure 4.7 continues

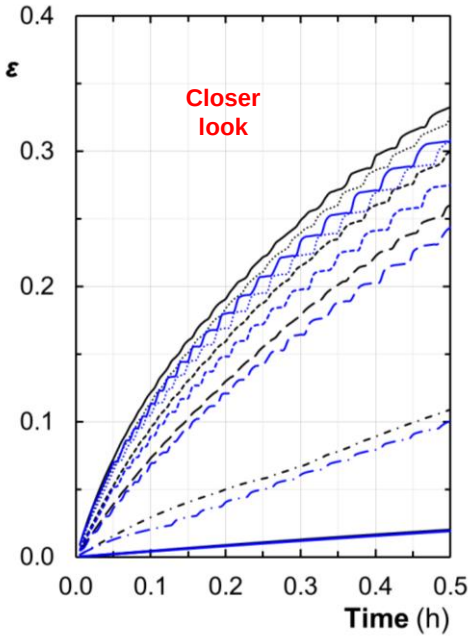

(b)

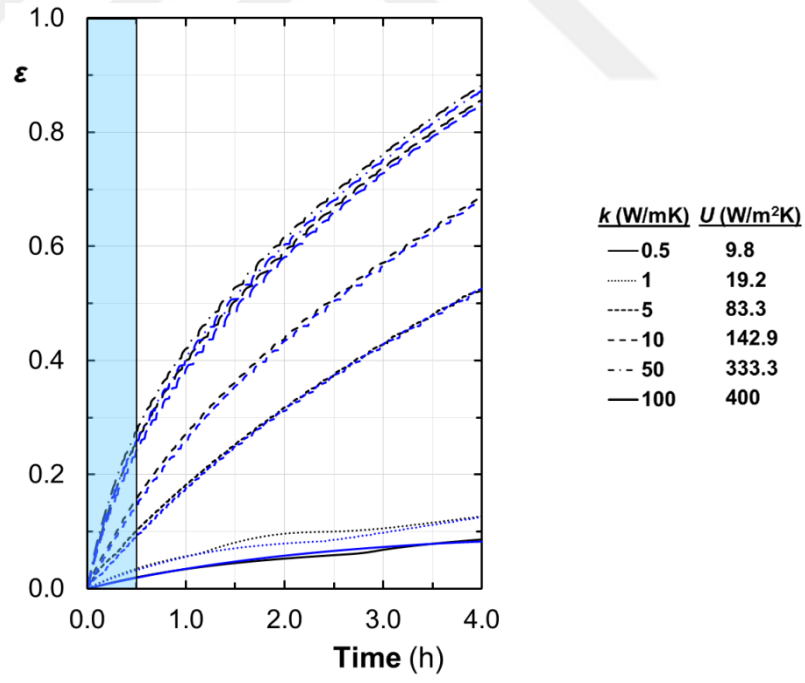

(a)

Figure 4.8 a) Effect of thermal conductivity on effectiveness, Side Cooling Without (blue) and with (black) natural convection b) closer look

Figure 4.8 continues

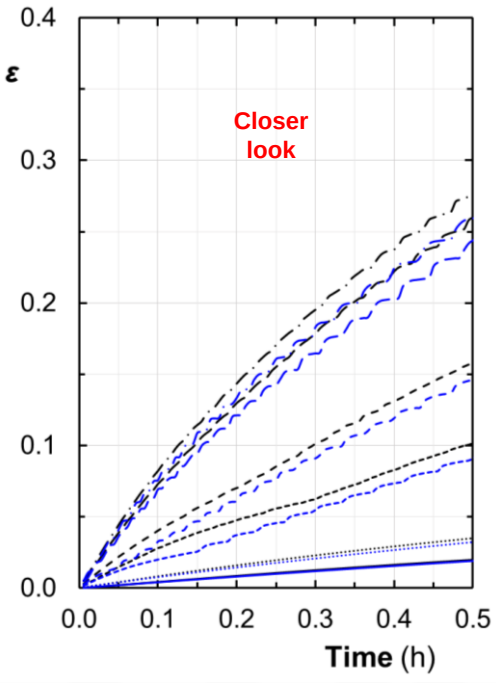

(b)

4.3.2 Bottom Cooling

Time-wise variations of bottom wall temperature are given in Figures 4.9 and 4.10, depending on the convective heat transfer coefficient of the outer surface and the thermal conductivity of the wall material, respectively. Analyses have been conducted for the same parameters as in the side cooling case, so the trends are look alike. The variation of bottom wall temperature differs from the previous case only for the lower U values. It looks like the variations of temperatures are almost identical through 0.5 h for U values less than 20 W/m^{2}K. Beyond this, the curves differentiate. For U = 9.8 W/m^{2}K, the temperature variation inverses at T_{wall} = 2.0°C. On the other hand, for U = 9.8 W/m^{2}K, it looks like the temperature fluctuates around 2.0°C for almost one hour and then gradually decreases from 2.0°C to approximate the curve that corresponds to the conduction dominated case.

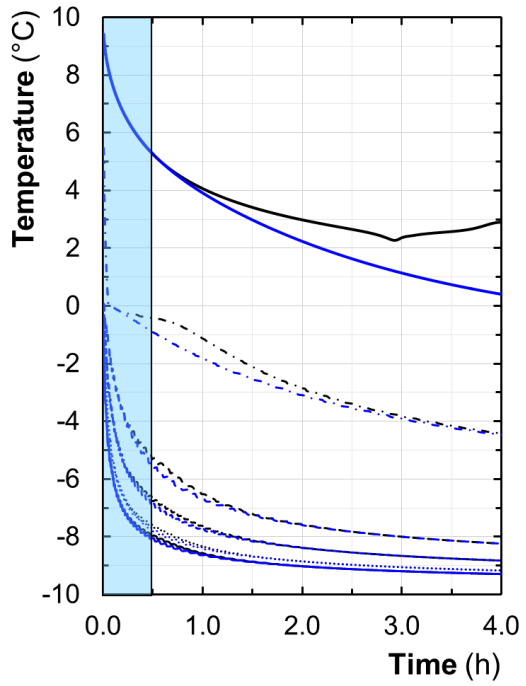

(a)

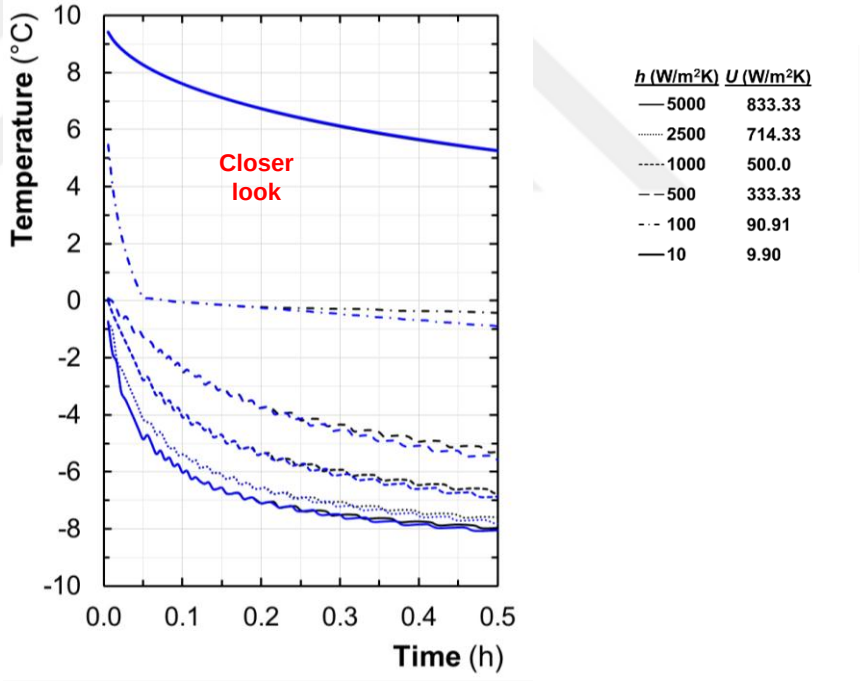

(b)

Figure 4.9 a) Effect of convective heat transfer coefficient on wall temperature, Bottom Cooling Without (blue) and with (black) natural convection b) closer look

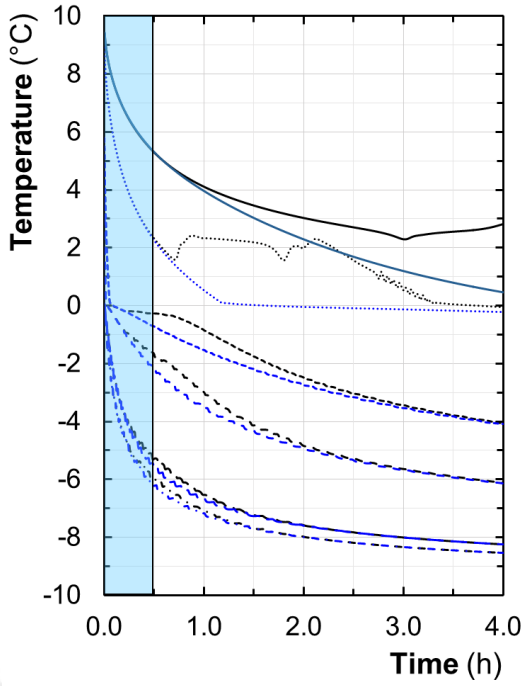

(a)

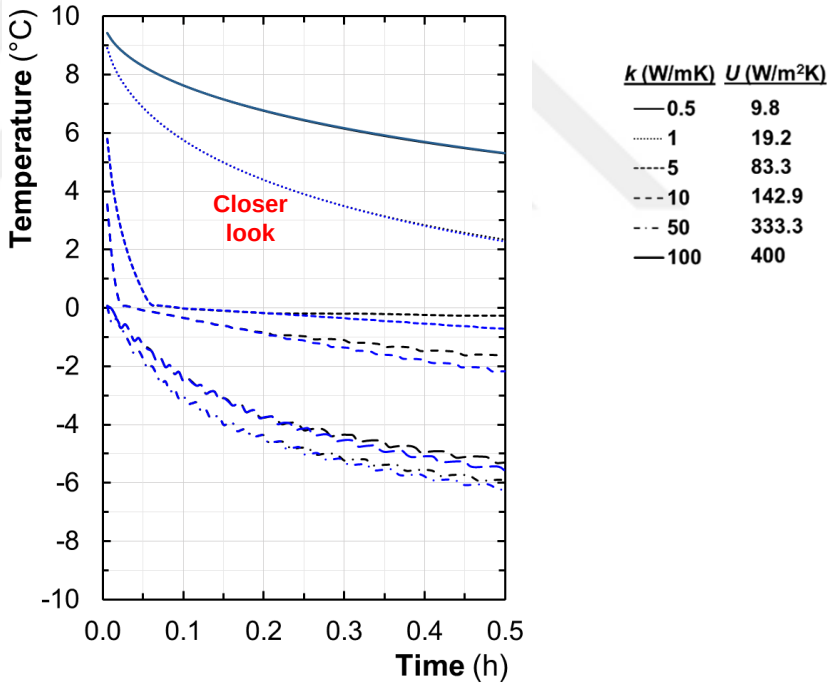

(b)

Figure 4.10 a) Effect of thermal conductivity on wall temperature, Bottom Cooling Without (blue) and with (black) natural convection b) closer look

Unexpected variation of the cold wall temperature for bottom cooling can be explained by analyzing the isotherms and streamlines. In conduction dominated case, Figure 4.11(a), isotherms are nearly horizontal. The heat gain through the walls slightly distorts the horizontal lines near the walls. In Figure 4.11(b), there is no significant change in convection dominated case until 600 s. Beyond that time, convection takes place and dominates the heat transfer inside the cavity. As seen in Figure 4.11(b), the domain is divided into two equal parts along the mid-width. In each part, there are two pairs of circulation cells around the density inversion line. The cold water moves from the interface through the upwards and forms four separate cells. The right-most cell rotates clockwise direction, and the cell close to it rotates in an anti-clockwise direction. In contrast, the left-most cell is in the anti-clockwise direction, and the cell near it rotates in clockwise direction. The convection currents bring hot water from the upper part of the cavity through the interface so that the bottom wall temperature could not drop through as quickly as in conduction dominated case.

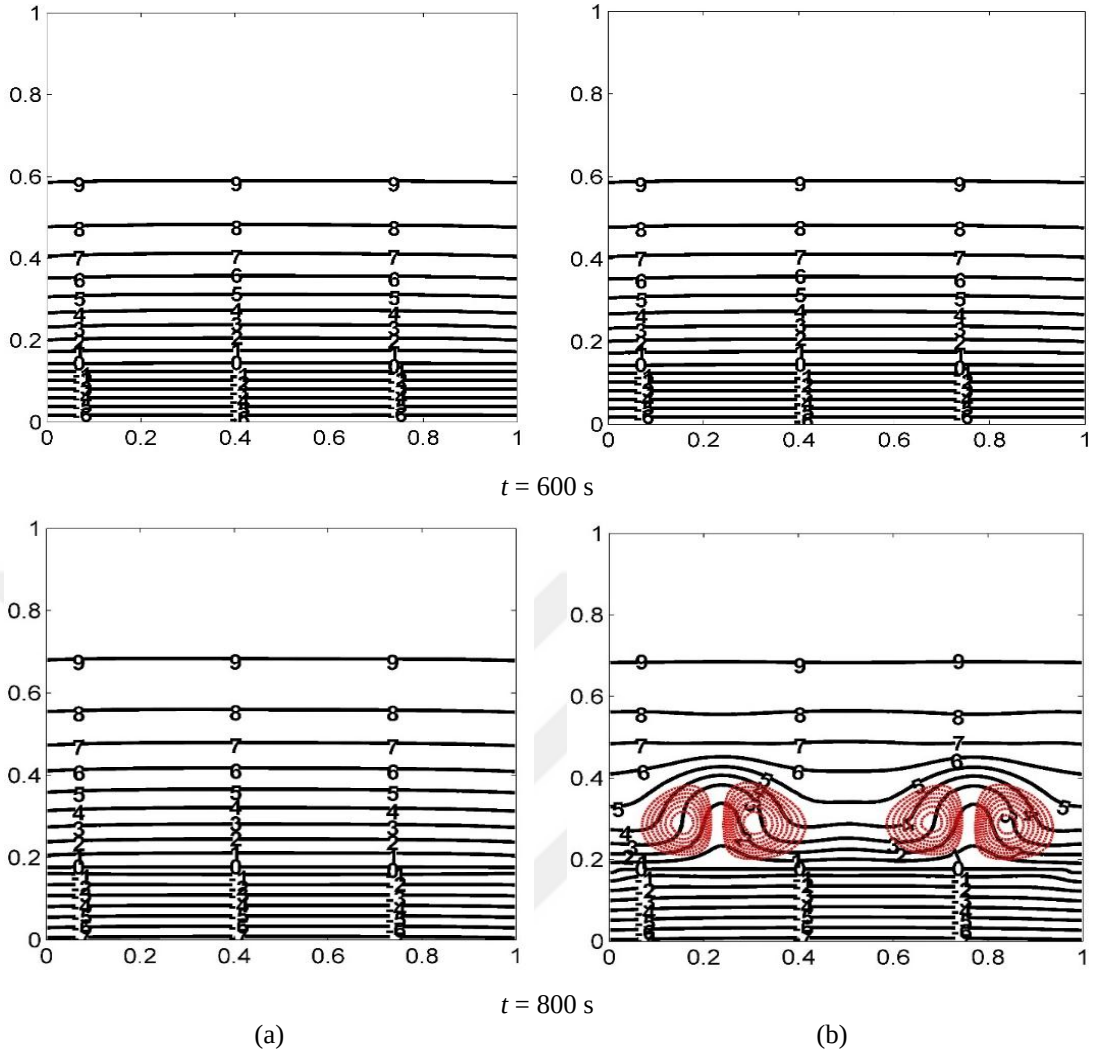

Figure 4.11 Temperature contours for a) Conduction and b) Convection dominated phase change, Bottom Cooling U = 833.33 W/m^{2}K

Figures 4.12 and 4.13 represent the influences of convective and conductive resistances on effectiveness. For lower *U*-values (< 20 W/m^{2}K), conduction dominated case is more effective than the convection dominated case. The effectiveness becomes identical for higher *U*-values. No significant difference is reported between the conduction and convection dominated cases for *U* values greater than 142.9 W/m^{2}K. The effectiveness increases almost ten times with increasing the *U* value from 9.9 to 90.91 W/m^{2}K. For higher *U*-values, on the other hand, the increments become marginal. By increasing the overall heat transfer coefficient from 400 W/m^{2}K to 833.33 W/m^{2}K, the increment regarding the effectiveness is only 7%. Results reveal that moderate heat transfer coefficients can

be used to achieve higher effectiveness with fewer convection coefficients or nominal thermal conductivities.

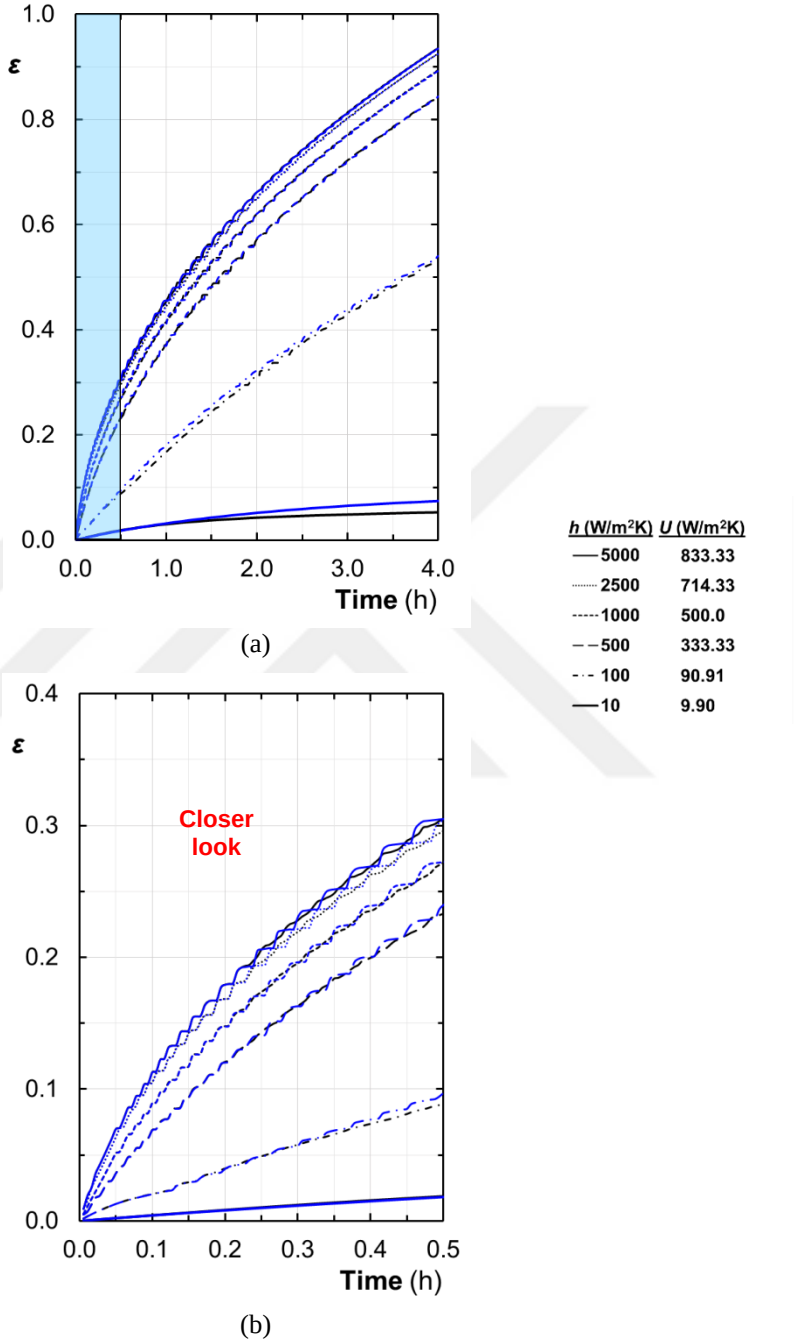

Figure 4.12 a) Effect of convective heat transfer coefficient on effectiveness, Bottom Cooling Without (blue) and with (black) natural convection b) closer look

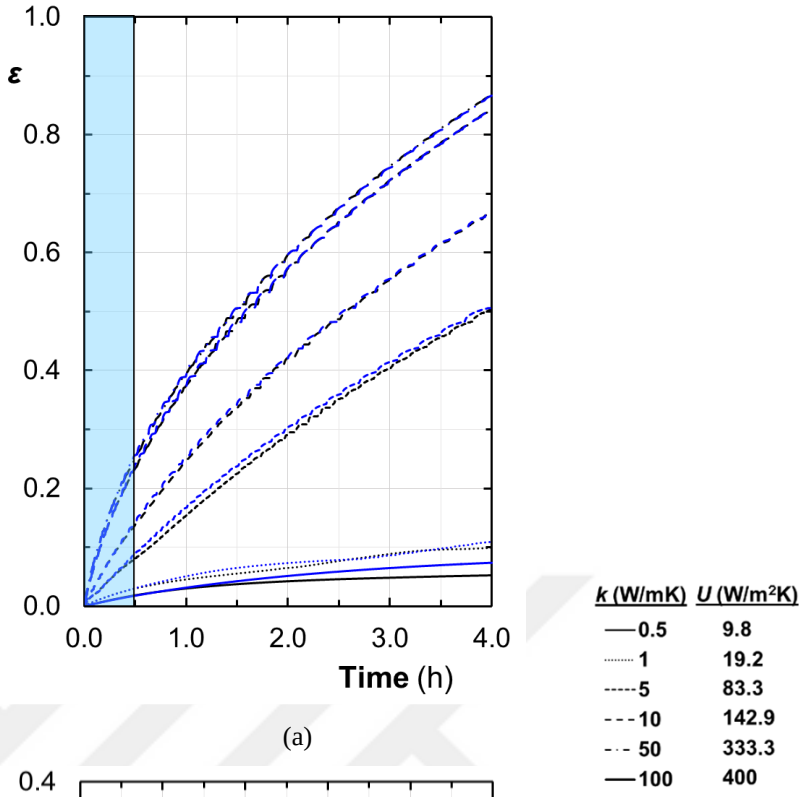

(a)

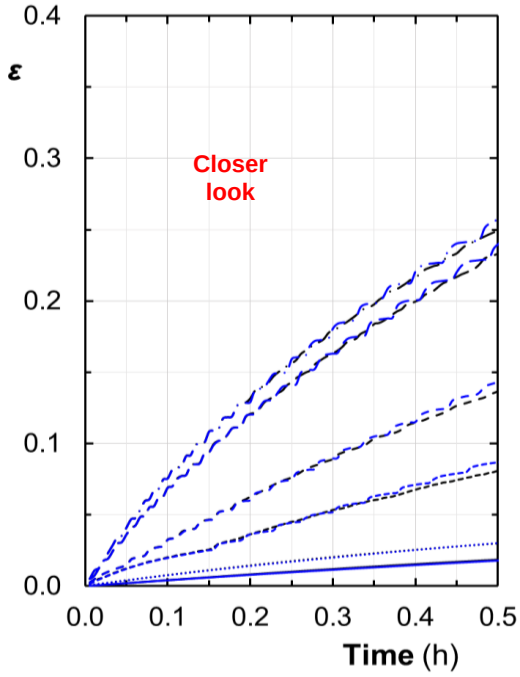

(b)

Figure 4.13 a) Effect of thermal conductivity on effectiveness, Bottom Cooling Without (blue) and with (black) natural convection b) closer look

4.3.3 Top Cooling

As a final case, cooling on top wall is investigated. Variations of the cold wall temperature are represented in Figures 4.14 and 4.15 for various convective heat transfer coefficients and thermal conductivities of the wall, respectively. Unlike the side and bottom wall cases, the transient behavior of the wall temperature looks more complex, especially for lower *U* values, in convection dominated case. The temperatures fluctuate at the initial periods, and the variations become smooth when the temperature drops below zero values. On the other hand, temperature variations look almost identical with the top cooling case when the convection effects are neglected. The buoyancy effects inside the cavity slow down the temperature variation of the cold wall. Even though there is a sharp difference between the conduction and convection dominated cases, the curves matches when the ice forms on the cold wall.

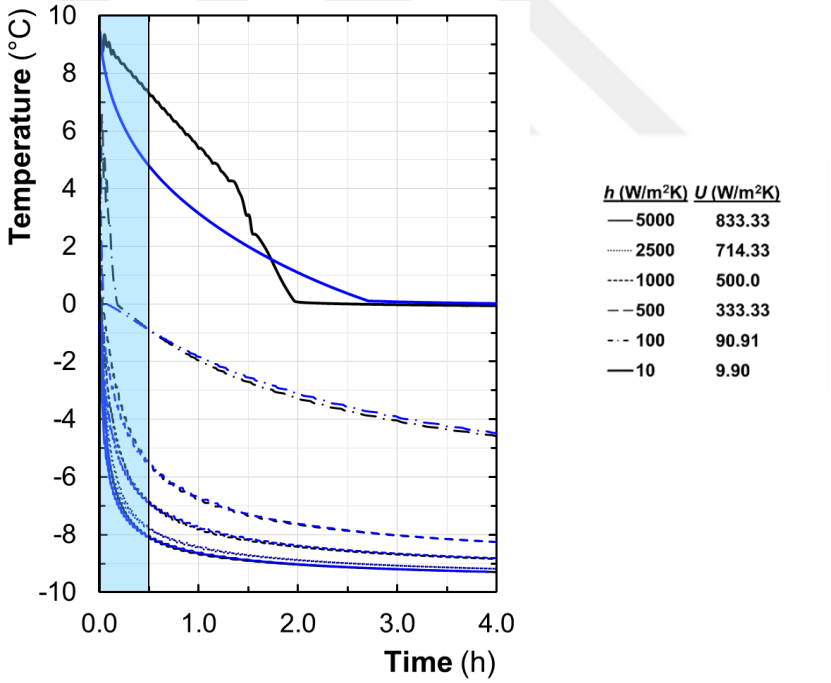

(a)

Figure 4.14 a) Effect of convective heat transfer coefficient on wall temperature, Top Cooling Without (blue) and with (black) natural convection b) closer look

Figure 4.14 continues

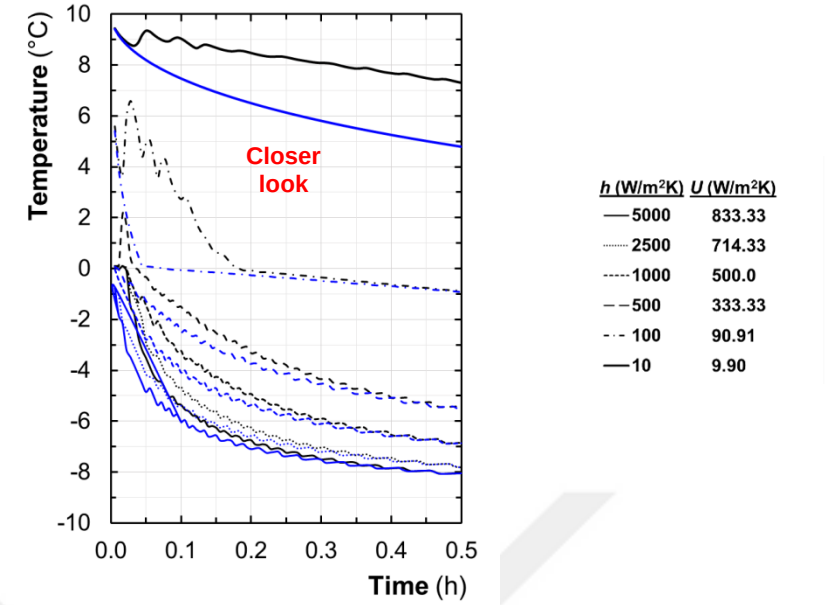

(b)

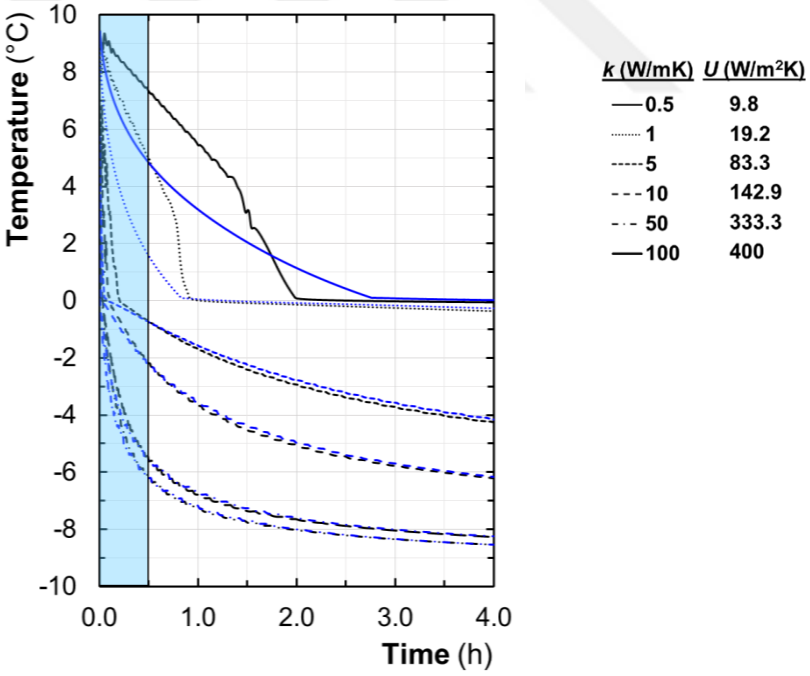

(a)

Figure 4.15 a) Effect of thermal conductivity on wall temperature, Top Cooling Without (blue) and with (black) natural convection b) closer look

Figure 4.15 continues

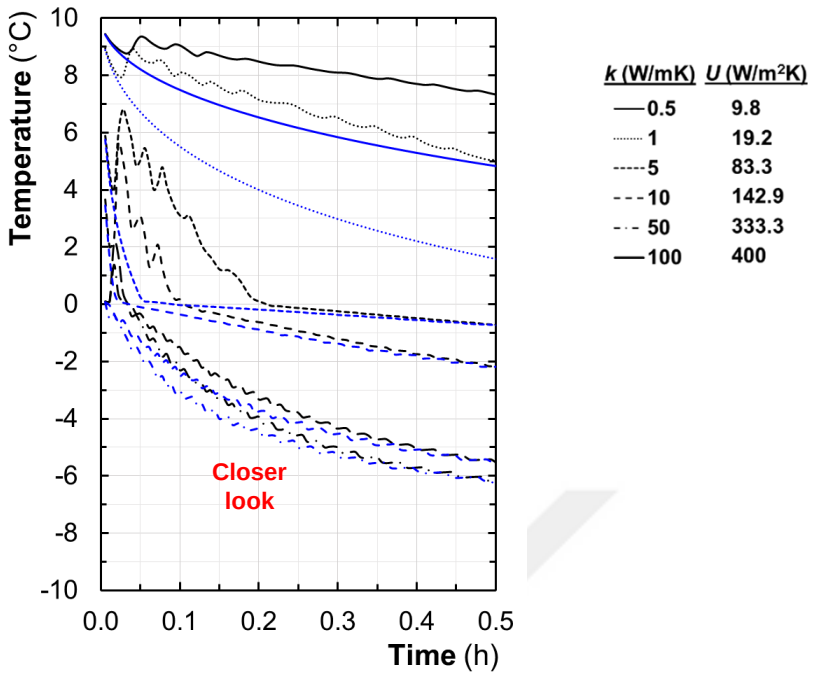

(b)

In Figure 4.16, the isotherms and streamlines are represented at t = 50 s and 1000 s for U = 833.33 W/m^{2}K. In conduction dominated case (Figure 16a), isotherms are almost horizontal, and the process has a harmony. Quite complicated isotherms are observed for natural convection driven phase change at t = 50 s. It appears four separate circulation cells at the upper-most of the cavity. While the hot water moves upward from the mid-line, cold water with higher density drops down and generates two thermal-plumes. Intense temperature gradients designate that the heat transfer rate is greater in the middle of the cavity. It is clear that the effect of buoyancy force increases the cooling rate of water. Nevertheless, at t = 1000 s, the ice thickness looks alike for conduction and convection dominated situations. The main difference between conduction and natural convection driven cases is that the average water temperature is nearly half for the case in which the buoyancy effect is included.

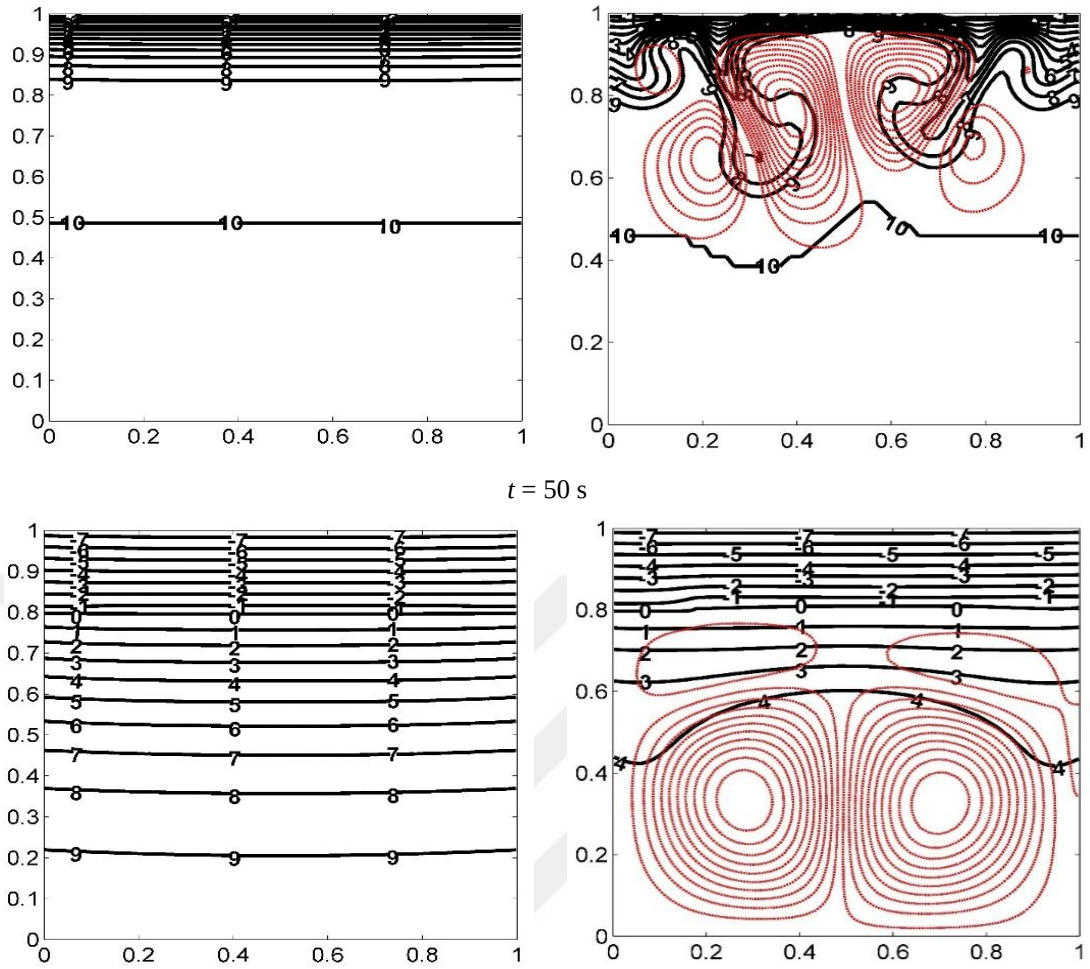

Figure 4.16 Temperature contours for (a) Conduction and (b) Convection dominated phase change Top Cooling, U = 833.33 W/m^{2}K

Figures 4.17 and 4.18 represent the effect of convective heat transfer and thermal conductivity on effectiveness. For relatively lower *U* values (< 20 W/m^{2}K), the convection dominated case looks more effective than the conduction dominated case. Unlike the previous cases, the effect of buoyancy force increases the effectiveness even for higher *U*-values in top cooling case. The difference between the conduction and convection dominated ones is remarkable during the initial periods. One can notice that the natural convection driven case is more effective than the conduction driven case for t < 0.5 h. The difference between the conduction and convection dominated ones becomes large for higher *U*-values. Increasing the overall heat transfer coefficient from 9.8 to 83.3 W/m^{2}K, the effectiveness enhances by five

times. Results also indicate that the effectiveness does not change significantly for U values greater than 333.33 W/m^{2}K.

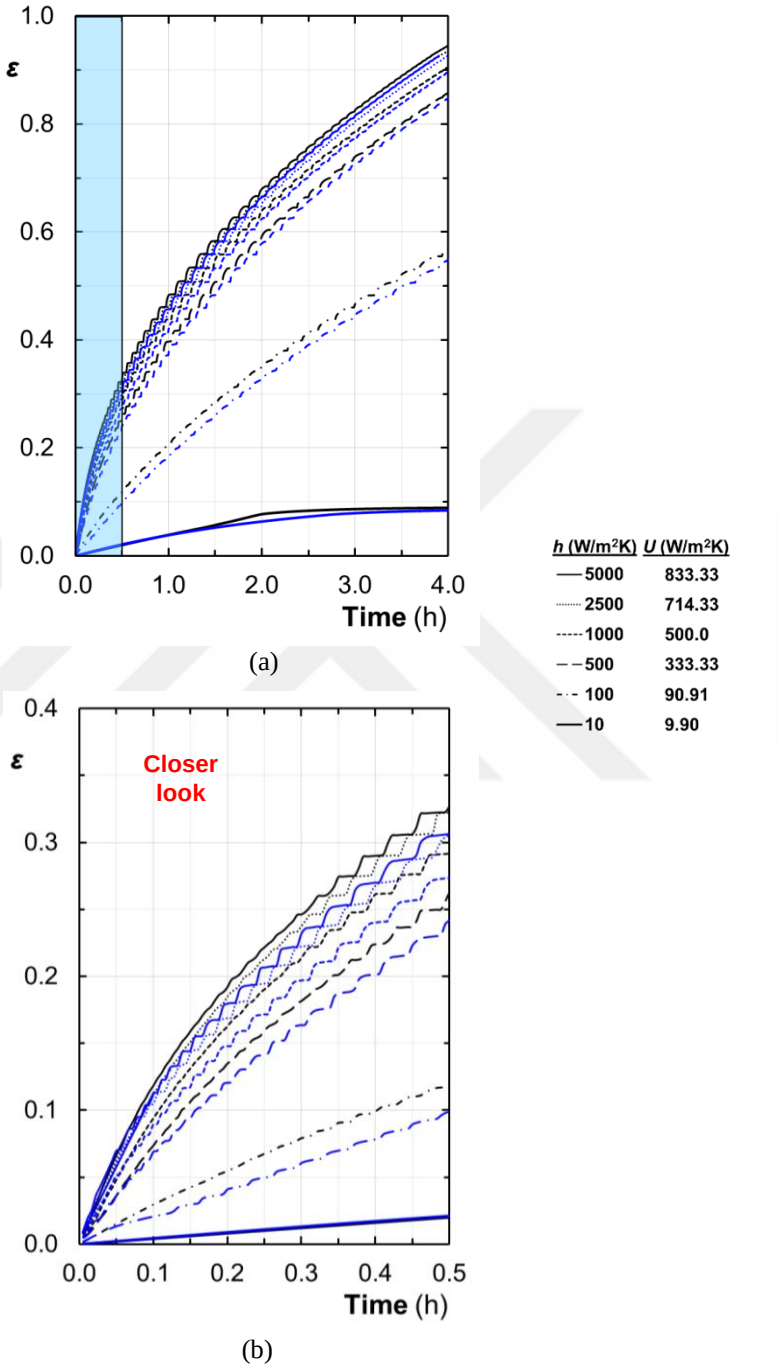

(a)

(b)

Figure 4.17 a) Effect of convective heat transfer coefficient on effectiveness – Top Cooling Without (blue) and with (black) natural convection b) closer look

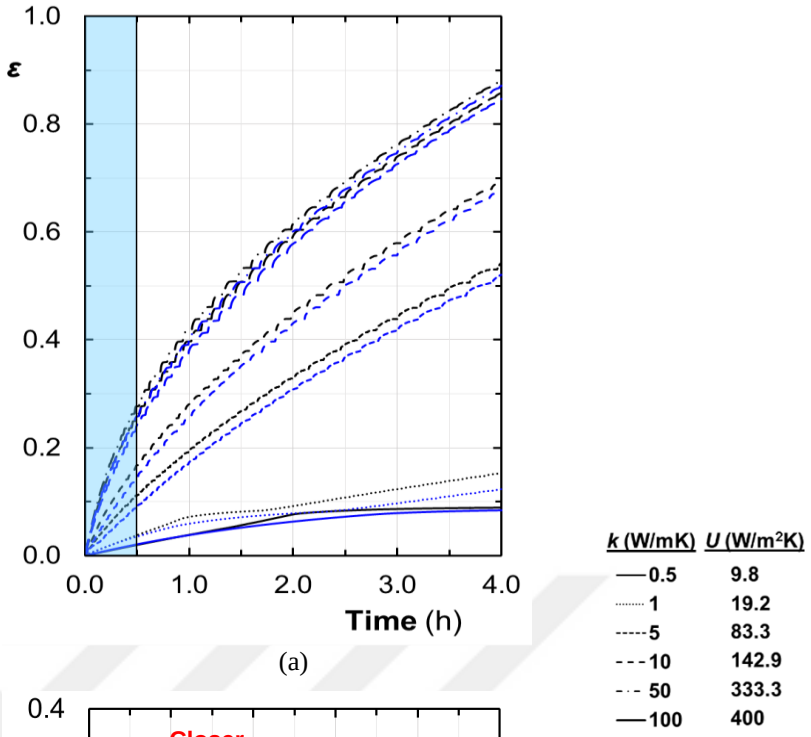

(a)

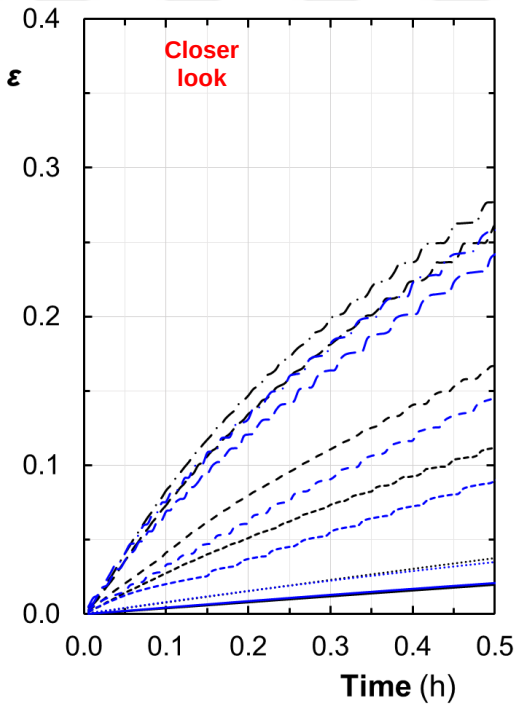

(b)

Figure 4.18 a) Effect of thermal conductivity on effectiveness, Top Cooling Without (blue) and with (black) natural convection b) closer look

CHAPTER FIVE
CONCLUSIONS

In this work, two types of transient natural convection problems in Cartesian coordinates are investigated numerically under different thermal boundary conditions and different aspect ratios. The results of the numerical analyses have also been validated with the experimental measurements from the literature.

The first problem of this study investigates the transient natural convection of water near its density inversion in a Cartesian geometry under different thermal boundary conditions and aspect ratios. The main outcomes of the numerical analyses are as follows;

- Considering a square cavity with side walls of T_c = 0°C and T_h = 8°C, two identical circulation cells by opposite directions are reported in the literature. In the current model, thermo-physical properties of water (i.e. density, viscosity, and thermal conductivity) are defined as a function of temperature. So that, the transient heat transfer near the cold and hot wall do not proceed symmetrically. Because of that, unlike the literature, asymmetric circulation cells are observed for R = 0.5.

- For H/W > 1, the counter-clockwise circulation cell dominates the domain. Besides, for H/W < 1, the flow field approaches to the symmetry, as the counter-clockwise circulation cell shifts the density inversion line from the mid-line through the cold wall.

- For partial cooling and heating conditions, similar behaviors are observed disregarding the aspect ratio of the cavity. It is clear that heating from the upper half of the wall is not an efficient way. Secondary circulation cell would not grow through the cold wall. This can only be effective in a small area which is close to the hot wall. On the other hand, heating from the lower part of the wall enhances

the heat transfer. The counter-clockwise circulation grows rapidly and become dominant for the entire domain at the steady state condition.

The last problem of this study considers the transient heat transfer process of freezing of water near its density inversion in a Cartesian geometry under different thermal boundary conditions. Solidification from the side, bottom, and top walls are compared with respect to the time-wise variation of the cold wall, isotherms, streamlines and energetic effectiveness, respectively. Analyses have been carried out for two major physics: conduction and natural convection. Comparative results made it possible to state that the influence of natural convection during phase change. The main consequences of the numerical analyses are listed as;

- Natural convection is significant during the initial periods of the phase change. Circulation cells have their own specific forms on the side, bottom, and top cooling cases.

- In early stages, the interface positions are different by both conduction and convection dominated cases. In advancing time, the interface positions are almost matched.

- Natural convection in the cavity increases the cooling rate of water. The average temperature of the water drops down quickly where the case that buoyancy forces are taken into account.

- Effectiveness is strongly affected by the overall heat transfer coefficient of the wall. The *U* values are more effective over 333.33 W/m^2K. The difference between the convection and conduction dominated processes becomes significant for top and side cooling cases.
- Near the density inversion temperature (4°C), natural convection strongly governs the solidification of water. Heat transfer may cause erroneous predictions especially considering the early stages of the process when the problem is reduced into conduction.

REFERENCES

Banaszek, J., Jaluria, Y., Kowalewski, T. A., & Rebow, M. (1999). Semi-implicit FEM analysis of natural convection in freezing water. Numerical Heat Transfer: Part A: Applications, *36*(5), 449-472.

Bergman, T. L., Incropera, F. P., & Lavine, A. S. (2011). Fundamentals of Heat and Mass Transfer. New York, John Wiley & Sons.

Blaszczuk, A. (2013). Experimental investigation of natural convection inside a upper part of vertical converging air channel using schlieren technique. Experimental Thermal and Fluid Science, *50*, 178–186.

Boger, D. V., & Westwater, J. W. (1967). Effect of buoyancy on the melting and freezing process. Journal of Heat Transfer, *89*, 81-89.

Braga, S. L., & Viskanta, R. (1992). Transient natural convection of water near its density extremum in a rectangular cavity. International Journal of Heat and Mass Transfer, *35*(4), 861-875.

Cao, Y., & Faghri, A. (1990). A numerical analysis of phase-change problems including natural convection. Journal of Heat Transfer, *112*(3), 812-816.

Cheikh, N.B., Beya, B.B., & Lili, T. (2007). Influence of thermal boundary conditions on natural convection in a square enclosure partially heated from below. International Communications in Heat and Mass Transfer, *34*, 369–379.

Chellaiah, S., & Viskanta, R. (1989). Freezing of water saturated porous media in the presence of natural convection: Experiments and analysis. Journal of Heat Transfer, *111*, 425-432.

Chen, T.H., & Chen, L.Y. (2007). Study of buoyancy-induced flows subjected to partially heated sources on the left and bottom walls in a square enclosure. International Journal of Thermal Sciences, *46*, 1219–1231.

Cheng, K. C., Inaba, H., & Gilpin, R. R. (1988). Effect of natural convection on ice formation around an isothermally cooled horizontal cylinder. International Journal of Heat and Mass Transfer, *110*, 931-937.

Chu, H.S.S., Churchill, S.W., & Patterson, S.V. (1976). The effects of heater size, location, aspect ratio and boundary conditions on two-dimensional, laminar, natural convection in rectangular channels. Journal of Heat Transfer, *98*, 194–201.

Deng, Q.H. (2008). Fluid flow and heat transfer characteristics of natural convection in square cavities due to discrete source-sink pairs positions. International Journal of Heat and Mass Transfer, *51*, 5949–5957.

DeVahl Davis, G. (1983). Natural convection of air in a square cavity; a bench mark numerical solution. International Journal of Numerical Methods of Fluids, *3*:249–264.

DeVahl Davis, G. & Jones, I.P. (1983). Natural convection in a square cavity: a comparison exercise. International Journal of Numerical Methods of Fluids, *3*:227–248.

Ezan, M.A. (2006). Design and optimization of ice-on-coil latent thermal storage system. M.Sc. Thesis, *Dokuz Eylül University,* İzmir.

Fusegi, T., & Hyun, J.M. (1994). Laminar and transitional natural convection in an enclosure with complex and realistic conditions. *International Journal of Heat and Fluid Flow, 15*(4):258–268.

Hale, N. W., & Viskanta, R. (1984). Solid-liquid phase-change heat transfer and interface motion in materials cooled or heated from above or below. *International Journal of Heat and Mass Transfer, 23*, 283-292.

Ho, C. J., & Viskanta, R. (1984). Inward solid-liquid phase-change heat transfer in a rectangular cavity with conducting vertical walls. International Journal of Heat and Mass Transfer, *27*(7), 1055-1065.

Hossain, M. A., & Rees, D. S. (2005). Natural convection flow of water near its density maximum in a rectangular enclosure having isothermal walls with heat generation. Heat and Mass Transfer, *41*(4), 367-374.

Inaba, H., & Fukuda, T. (1984). Natural convection in an inclined square cavity in regions of density inversion of water. Journal of Fluid Mechanics, *142*, 363-381.

Jin, W.W., Tao, W.Q., He, Y.L., & Li, Z.Y. (2008). Analysis of Inconsistency of SIMPLE-like Algorithms and an Entirely Consistent Update Technique - The CUT Algorithm. Numerical Heat Transfer, Part B: Fundamentals: An International Journal of Computation and Methodology.

Kandaswamy, P., Sivasankaran, S., & Nithyadevi, N. (2007). Buoyancy-driven convection of water near its density maximum with partially active vertical walls. International Journal of Heat and Mass Transfer, *50*(5), 942-948.

Lankford, K. E., & Bejan, A. (1986). Natural convection in a vertical enclosure filled with water near 4°C. Journal Heat Transfer, *108*, 755-763.

Lee, SL. (1989). A strongly implicit solver for two–dimensional elliptic differential equations. Numerical Heat Transfer, *16*, 161–178.

Lin, D. S., & Nansteel, M. W. (1987). Natural convection heat transfer in a square enclosure containing water near its density maximum. International Journal of Heat and Mass Transfer, *30*(11), 2319-2329.

McDonough, M. W., & Faghri, A. (1994). Experimental and numerical analyses of the natural convection of water through its density maximum in a rectangular enclosure. International Journal of Heat and Mass Transfer, *37*(5), 783-801.

Moraga, N. O., & Vega, S. A. (2004). Unsteady three-dimensional natural convection of water cooled inside a cubic enclosure. Numerical Heat Transfer, Part A: Applications, *45*(8), 825-839.

Muralidhar, K., Patil, V.B., & Kashyap, R. (1995). Interferometric study of transient convection in a square cavity. Journal of Flow Visualization and Image Processing, *2*, 321–333.

Nithyadevi, N., Sivasankaran, S., & Kandaswamy, P. (2007). Buoyancy-driven convection of water near its density maximum with time periodic partially active vertical walls. Meccanica, *42*(5), 503-510.

Nithyadevi, N., Kandaswamy, P., & Lee, J. (2007). Natural convection in a rectangular cavity with partially active side walls. International Journal of Heat and Mass Transfer, *50*(23), 4688-4697.

Patankar, S.V. (1980). Numerical heat transfer and fluid flow. New York, McGraw-Hill.

Ravi, M.R., Henkes, R.A.W.M., & Hoogendoorn, C.J. (1994). On the high-Rayleigh-number structure of steady laminar natural convection flow in a square enclosure. Journal of Fluid Mechanics, *262*:325–351.

Seki, N. (1978). Free convective heat transfer with density inversion in a confined rectangular vessel. Wärme-und Stoffübertragung, *11*(3), 145-156.

Sharif, M.A.R., & Mohammad, T.R. (2005). Natural convection in cavities with constant flux heating at the bottom wall and isothermal cooling from the sidewalls. International Journal of Thermal Sciences, *44*, 865–878.

Shiralkar, G., Gadgil, A., & Tien, C.L. (1981). High Rayleigh number convection in shallow enclosures with different end temperatures. International Journal of Heat and Mass Transfer, *24*(10):1621– 1629.

Sugawara, M., Inaba, H., & Seki, N. (1988). Effect of maximum density of water on freezing of a water-saturated horizontal porous layer. Journal of Heat Transfer, *110*, 155-159.

Turkoglu, H., & Yucel, N. (1995). Effects of heater and cooler location on natural convection in square cavities. Numerical Heat Transfer, Part A: Applications, *27*, 351–358.

Valencia, A., & Frederick, R.L. (1989). Heat transfer in square cavities with partially active vertical walls. International Journal of Heat and Mass Transfer, *8* (32), 1567–1574.

Versteeg, H.K., & Malalasekara, W. (1995). An introduction to computational fluid dynamics: The finite volume method. New York, Pearson Education.

Wang, S., Faghri, A., & Bergman, T.L. (2010). A comprehensive numerical model for melting with natural convection. International Journal of Heat and Mass Transfer, *53*, 1986–2000.

Wei, T., & Koster, J. N. (1994). Density inversion effect on transient natural convection in a rectangular enclosure. International Journal of Heat and Mass Transfer, *37*(6), 927-938.

Wu, W., & Ching, C.Y. (2010). Laminar natural convection in a square cavity with a portion on the heated vertical wall. Experimental Heat Transfer, *32*, 298–316.

Yewell, R., Poulikakos, D., & Bejan, A. (1982). Transient natural convection experiments in shallow enclosures. Journal of Heat Transfer, *104*, 533 538.

Zaman, F.S., Turja, T.S., & Molla, M. (2013). Buoyancy driven natural convection flow in an enclosure with two discrete heating from below. Procedia Engineering, *56*, 104–111.

Zhao, F.H., Liu, D., & Tang, G.F. (2007). Resonant response of fluid flow subjected to discrete heating elements. Energy Conversion and Management, *48*, 2461–2472.

APPENDICES

Nomenclature

A	Area, m^2
c	Specific heat, $Jkg^{-1}K^{-1}$
C	Heat capacity, Jm^{-3}
g	Gravitational acceleration, ms^{-2}
h	Convective heat transfer coefficient, $Wm^{-2}K^{-1}$
H	Height of cavity, m, enthalpy, Jkg^{-1}
k	Thermal conductivity, $Wm^{-1}K^{-1}$
Nu	Nusselt number
p	Pressure, Pa
R	Density inversion parameter
t	Time, s
T	Temperature, °C, K
u, v	Velocity components, ms^{-1}, mms^{-1}
U	Overall heat transfer coefficient, $Wm^{-2}K^{-1}$
W	Width of the cavity, m
x, y	Coordinates, m
X	Dimensionless horizontal coordinate, x/H
Y	Dimensionless vertical coordinate, y/H
S	Source term, Jm^{-3}

Greek Symbols

ε	Effectiveness
δT	Mushy range temperature, °C
ϕ	Variable
θ	Dimensionless temperature, $(T - T_C)/(T_H - T_C)$
ξ	Height of the active wall, m
ρ	Density, kgm^{-3}

μ	Dynamic viscosity, $kgm^{-1}s^{-1}$

Subscripts

c	Cold
in	Initial
l	Liquid
m	Maximum density, melting, mushy
ref	Reference
s	Solid
sf	Solid-liquid
∞	Ambient

SIMPLE Algorithm

```
Xmom_Coefficients();
SIS(U, AP_U, SU, AN_U, AS_U, AE_U, AW_U, N, M);
Ymom_Coefficients();
SIS(V, AP_V, SV, AN_V, AS_V, AE_V, AW_V, N, M);
Pressure_Correction_Coefficients();
SIS(P1, AP_P, SP, AN_P, AS_P, AE_P, AW_P, N, M);
Pressure_Velocity_Correction();
Faghri();
Energy_Coefficients();
SIS(T, AP_T, ST, AN_T, AS_T, AE_T, AW_T, N, M);
Convergence_Check();
```

CUT Algorithm

```
Xmom_Coefficients();
Ymom_Coefficients();
Explicit_velocity();
Pressure_Correction_Coefficients();
SIS(P1, AP_P, SP, AN_P, AS_P, AE_P, AW_P, N, M);
Pressure_Velocity_Correction();
Faghri();
Energy_Coefficients();
SIS(T, AP_T, ST, AN_T, AS_T, AE_T, AW_T, N, M);
Convergence_Check();
```